Alma Mater Studiorum · Università di Bologna

Scuola di Scienze
Corso di Laurea Magistrale in Fisica

Turbulence models in the Atmospheric Boundary Layer under convective conditions

Relatore:
Prof. Francesco Tampieri

Correlatore:
Dott. Alberto Maurizi

Presentata da:
Olimpia Bruno

Sessione III
Anno Accademico 2012/2013

A Demetrio,
ai miei zii Nino e Olimpia e ai miei genitori.

Abstract

In questo lavoro viene effettuata una modellizzazione della turbolenza nello strato limite atmosferico, in condizioni convettive. A tal fine, le equazioni che descrivono il moto dell'atmosfera vengono espresse attraverso medie alla Reynolds e necessitano, dunque, di chiusure.
Tale lavoro consiste nel modificare la chiusura TKE-l usata nel modello di previsione meteorologica BOLAM (Bologna Limited Area Model). In particolare, viene utilizzato il modello colonnare del BOLAM, il quale viene modificato in modo da ottenere tre ulteriori schemi di chiusura: alle relazioni flusso-gradiente usate per chiudere i momenti secondi dell'equazione di evoluzione della energia cinetica turbolenta viene sommato un termine non locale, in modo da rendere la relazione flusso-gradiente più idonea per simulare uno strato limite instabile.
Inoltre viene effettuato un confronto tra i risultati ottenuti dal modello colonnare, quelli ottenuti dai nuovi tre schemi e le osservazioni fornite dal caso noto in letteratura come "GABLS2".

Abstract

In this work a modelization of the turbulence in the atmospheric boundary layer, under convective condition, is made. For this aim, the equations that describe the atmospheric motion are expressed through Reynolds averages and, then, they need closures.
This work consists in modifying the TKE-l closure used in the BOLAM (Bologna Limited Area Model) forecast model. In particular, the single column model extracted from BOLAM is used, which is modified to obtain other three different closure schemes: a non-local term is added to the flux-gradient relations used to close the second order moments present in the evolution equation of the turbulent kinetic energy, so that the flux-gradient relations become more suitable for simulating an unstable boundary layer. Furthermore, a comparison among the results obtained from the single column model, the ones obtained from the three new schemes and the observations provided by the known case in literature "GABLS2" is made.

Introduction

In the study of the atmosphere, an important role is played by the atmospheric boundary layer. This concept was, probably for the first time, introduced by Prandtl (1905) and can be described as the layer closest to the Earth's surface, in which the effect of friction, heating and cooling is felt, and in which fluxes of momentum, heat and matter are significant. The equations of motion of the atmosphere are the Navier-Stokes equations. Anyhow, every variables characterizing the atmosphere can be considered, thanks to the Reynolds decomposition, as the sum of a mean term and a fluctuating term. Applying this Reynolds decomposition to the Navier-Stokes equations, the Reynolds Averaged Navier-Stokes (RANS) equations are obtained. These equations, however, have second order moments (that represent fluxes) which must be solved and, then, need some closures. Different ways exist to close the equations in question and it depends on the closure order that you want to use. If the closure used is at the first order, it is the so-called flux-gradient relation: the flux of a variable along a direction is directly proportional to the gradient of the variable in question along the same direction of the flux (in analogy with the Fick's low).

In this work a convective boundary layer (CBL) is simulated using a single column model (SCM), which is part of the BOLAM (Bologna Limited Area Model) forecast model. In the SCM the horizontal homogeneity approximation is used and it simplifies the evolution equations of the fluid. The closure used in the SCM is a second order closure on the turbulent kinetic energy (TKE), in which the second order moments are processed with the flux-gradient relation and the third order moments are solved with the inversion of a tridiagonal matrix. To simulate a CBL, the case "GABLS2" is considered for the initial and the boundary conditions, that consist in an initial vertical profile of the potential temperature θ, a prescribed geostrofic wind at the top of the layer and a prescribed time evolution of the temperature at the ground. Anyhow, the use of the flux-gradient relation is not a good solution in a CBL simulation, then a modified flux-gradient relation is introduced, in which a non-local term is added to the local one. In particular, three different schemes are proposed in this work to

study how much they contribute in the SCM, where the non-local terms are taken by Holtslag and Boville (1993) (for the heat flux), Frech and Mahrt (1995) and Brown et al. (2008) (these last two for the momentum fluxes). The results obtained by the three different schemes are compared with the results obtained by the original SCM and the observations provided by the case "GABLS2" (see Svensson et al. (2011)). Furthermore, different ways to compute the mixing height have been included in the SCM, to make a comparison among them.

Besides the main work of this thesis, an experiment based on the change of the vertical resolution of the SCM is made, to see the dependence of the integration in space of the equations of motion from it.

In Chapter 1, an introduction on the atmospheric boundary layer is presented, with a special attention on the convective boundary layer. This chapter, moreover, deals with theoretical outlines about the turbulence, the similarity theory and the flux-gradient relation. In Chapter 2, the equations of motion are treated, under the horizontal homogeneity approximation: in particular, it includes the description of the RANS equations, different ways to close them at different orders and a section dedicated to the different way to compute the mixing height. In Chapter 3, the used numerical models are described, together with the different closures used. In Chapter 4, the compare among the numerical results and the experimental observations is reported. The Appendix includes theoretical outlines about the Richardson number and the experiment based on the change of the vertical resolution.

This work has been performed at the institute ISAC-CNR in Bologna.

Contents

Chapter 1

Turbulence in the atmospheric boundary layer

1.1 Introduction to the atmospheric boundary layer

The concept of boundary layer was probably introduced in the literature for the first time by Prandtl (1905). In particular Prandtl, thanks to his work in the field of aerodynamics, recognized the transition from irrotational flow well away from the boundary to the condition of no-slip at the boundary.

In the atmospheric context, the boundary layer can be defined as the layer of air directly above the Earth's surface, in which effects like friction, heating and cooling are felt, and in which significant fluxes of momentum, heat or matter are carried by turbulent motions on a scale of the order of the depth of the boundary layer or less.

The atmospheric turbulence, involved in the atmospheric boundary layer (ABL), has two main features: turbulence associated with thermal convection coexists with mechanical turbulence (that is generated by wind shear); boundary layer (BL) turbulence interacts with a mean flow that is influenced by the rotation of the Earth.

It is possible to distinguish two region in the atmospheric boundary layer: the inner and the outer layer. In the outer layer, also called the Ekman layer, the flow shows only a little dependence on the nature of the surface, and the Coriolis force due to the

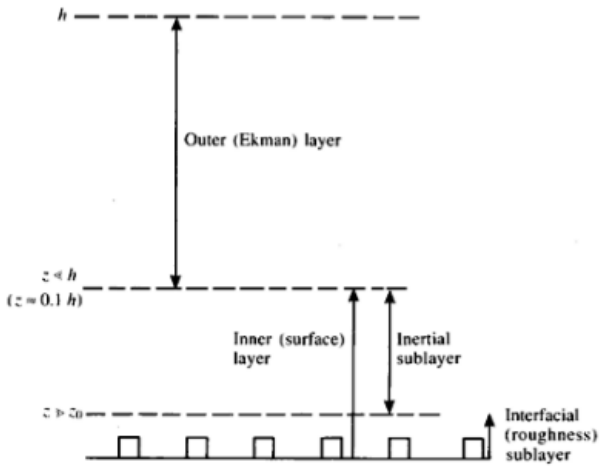

Figure 1.1: A scheme of atmospheric boundary layer taken from Garratt (1992)

Earth's rotation is important. In the inner layer the flow is mainly dependent on the surface characteristics and is little affected by rotation. In this layer a further classification is made: an interfacial sublayer is distinguishable than an inertial sublayer. The interfacial sublayer is directly influenced by the surface, because it is "the layer of air within and just above the roughness elements comprising the land or sea surface" (Garratt (1992)).

It is possible to have three types of boundary layer, because of its dependence on the sign of the vertical heat flux at the ground $\overline{w'\theta'}|_0$ (the zero subscript is an indication for values at the ground):

- stable boundary layer (SBL) if $\overline{w'\theta'}|_0<0$;
- unstable or convective boundary layer (CBL) if $\overline{w'\theta'}|_0>0$;
- neutral boundary layer (NBL) if $\overline{w'\theta'}|_0 = 0$.

where w' is the fluctuation of the vertical component of the wind speed and θ' is the fluctuation of the potential temperature (all the variables superscripted represents the fluctuation of the variable in question). The potential temperature is defined as:

$$\theta = T\left(\frac{p_0}{p}\right)^{\frac{R}{c_p}} \tag{1.1}$$

where T is the absolute temperature of the air volume considered, p_0 is a reference pressure (usually $1000Pa$), p is the pressure of the simple of air considered, R is the gas constant of air and c_p is the specific heat capacity at a constant pressure. So the potential temperature represents the temperature that an air parcel could have if, starting from a temperature T and a pressure p, it was adiabatically brought at pressure p_0. Anyhow, some informations will be given in detail later.

1.2 Turbulence and turbulent flows

Through the Reynolds number Re, it is possible to establish if a flow is laminar or turbulent. The Reynolds number is defined as $Re = \frac{UL}{\nu}$, where U and L are characteristic velocity and length scale of the flow, and ν is the kinematic viscosity of the fluid. In the Reynolds experiment the flow is laminar if Re<2300 ca and is turbulent if Re>4000 ca. At high Reynolds number there is a separation of scales: the large-scale motions are strongly influenced by the geometry of the flow and control the transport and the mixing; the small-scale motions are not influenced by the geometry of the flow but by the rate at which they receive energy from the large scales. In particular, in a turbulent flow, the large vortices obtain their energy from the anisotropy of the mean flow due to the turbulent flow itself; through a vortex stretching process this energy is transfered by large vortices to the smaller ones. The smaller vortices are dragged by the larger ones (that have the role of mean motion) because of their dimensions, so the smaller vortices don't interact with the mean motion and are isotropic. This transfer of energy happens until the dimension of the smaller vortices is small enough to be dissipated as heat. The viscosity is important to estimate the dimension at which this dissipation happens (ε is the viscosity dissipation):

$$l_{min} \sim \left(\frac{\nu^3}{\varepsilon}\right)^{\frac{1}{4}} \tag{1.2}$$

This process just described is called *energy cascade* and was introduced, for the first time, by Richardson. To have a better comprehension about what has just been said, it could be appropriate referring to the similarity theory.

1.2.1 The similarity theory of turbulence

The similarity theory was developed in 1941 by Kolmogorov and based on the concept of the energy cascade and the three-dimensional energy spectrum. In fact, at large Reynolds number the energy spectrum is wide as to decouple the turbulent structure from the original anisotropic form, with a consequent tendency to local isotropy in an equilibrium range of wavenumbers. In this equilibrium range the average properties of the small-scale components of any turbulent motion - at large Re - are determined uniquely by ν and ε, according to the equation (1.2).

In this way Kolmogorov defined, in the energy spectrum of turbulence, an inertial subrange. In this range the smaller vortices are isotropic and viscosity dissipation is not included (Fig. (1.2)).

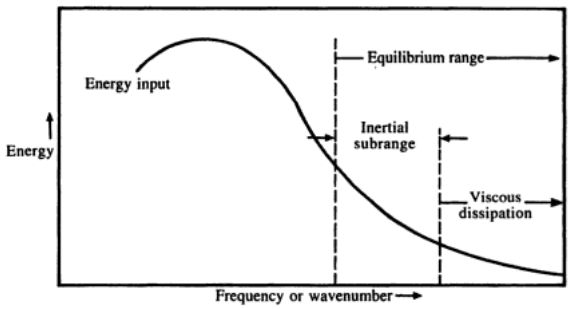

Figure 1.2: A scheme of energy spectrum in turbulence, taken from Garratt (1992)

1.2.2 Monin-Obukov similarity theory

Monin and Obukhov, in their theory (1954), hypothesized the presence of a scaling length L_{MO} for the surface layer (it will be discuss later what is the surface layer), defined as:

$$L_{MO} = -\frac{{u_*}^3}{\frac{kg}{\theta_{00}}\overline{w'\theta'}|_0} \tag{1.3}$$

where k is the von Kàrmàn constant and u_* is the friction velocity defined as:

$$u_* = \left(\overline{u'w'}|_0^2 + \overline{v'w'}|_0^2\right)^{\frac{1}{4}} \tag{1.4}$$

that is often used as velocity scale; $\overline{u'w'}|_0$, $\overline{v'w'}|_0$ and $\overline{w'\theta'}|_0$ are fluxes values for momentum (the first two) and for heat (the last one) at the ground. In this way, for example, to determine the CBL it has to be L_{MO}<0.

In the similarity theory it is expected that any dimensionless characteristics of the turbulence can depend only upon a dimensionless height $\zeta = \frac{z}{L_{MO}}$. In particular, it's possible to find a stability function Φ_M through the vertical gradient of the horizontal component of the wind $\frac{\partial u}{\partial z}$ scaled on $\frac{u_*}{kz}$:

$$\frac{kz}{u_*}\frac{\partial u}{\partial z} = \Phi_m(\zeta) \tag{1.5}$$

There is also a stability function related to the vertical gradient of the virtual potential temperature $\frac{\partial \theta}{\partial z}$, scaled on $\frac{\theta_*}{kz}$:

$$\frac{kz}{\theta_*}\frac{\partial \theta}{\partial z} = \Phi_h(\zeta) \tag{1.6}$$

where the temperature scale θ_* is defined as follows:

$$\theta_* = -\frac{\overline{w'\theta'}|_0}{u_*} \tag{1.7}$$

These stability functions have the following general form:

$$\Phi(\zeta) = 1 + \alpha_1\zeta + \alpha_2\zeta^2 + ... \simeq 1 + \alpha_1\zeta \tag{1.8}$$

where the final approximation is possible only for small values of ζ. In fact, because of dependence of ζ from L_{MO}, the parameter ζ is a measure of the influence of buoyancy, and for large values of $|L_{MO}|$ there are small values of $|\zeta|$ which make possible that approximation. From the integration of the equation (1.5), the velocity profile can be obtained:

$$\overline{u}(z) \simeq \frac{u_*}{k}\left(ln\frac{z}{z_0} + \alpha_m\frac{z - z_0}{L_{MO}}\right) \tag{1.9}$$

When $|L_{MO}| \to \infty$, $|\zeta| \to 0$ and $\Phi = 1$, the neutral case is obtained, in which there is a logarithmic vertical profile of the mean wind velocity given by:

$$\overline{u}\,(z) = \frac{u_*}{k} ln \frac{z}{z_0} \tag{1.10}$$

where z_0 is called the roughness height. However, in the case of the CBL the situation is different from that just described. In fact $\zeta \to -\infty$ and Monin-Obukhov scaling fails, so a detailed explanation will be treated in Section (1.3)

1.2.3 The flux-gradient relations

In analogy with the Fick law, it is used to relate the flux of a scalar (like θ) or of a vector component (like u or v) along a direction with its gradient in that same direction. In particular, the vertical direction is the most used (such as in our case, in which horizontal homogeneity is used to study the BL) and, considering the molecular property of transport, the relations most used are:

$$\overline{u'w'} = -K_m \frac{d\overline{u}}{dz} \tag{1.11}$$

$$\overline{v'w'} = -K_m \frac{d\overline{v}}{dz} \tag{1.12}$$

$$\overline{w'\theta'} = -K_h \frac{d\overline{\theta}}{dz} \tag{1.13}$$

$$\overline{w'q'} = -K_h \frac{d\overline{q}}{dz} \tag{1.14}$$

where q is the mixing ratio and K_m and K_h are coefficients of diffusivity. These coefficients are dimensionally equal to the product of a velocity and a length:

$$K = UL \tag{1.15}$$

From the equation (1.11), for example, it is possible to write K_m through a dimensional analysis:

$$K_m = \frac{-\overline{w'u'}}{\frac{d\overline{u}}{dz}} = \overline{w'l'} \tag{1.16}$$

where l' represents the fluctuation of the size of the vortex.

The square root of the variance of the vortex size fluctuation is called *mixing length* and it is an important length scale:

$$l_m = \sqrt{\alpha \overline{l'^2}} \tag{1.17}$$

The importance of the mixing length will be discuss later.

1.3 The convective boundary layer

The surface heating and cooling, together with the presence of clouds, strongly influence the structure of the ABL turbulence. In the case of CBL the surface heating drives unstable conditions and convective motions are established together with the formation of vortices vertically developed. The outer layer dominated by these motions is called mixed layer, because the strongest mixing phenomena are localized in that layer. The intermediate layer is dominated by convection and the surface layer, that includes not more than 10% of the total CBL, is influenced by the mechanical interaction with the ground. The top of the CBL is often defined by the presence of an inversion layer which does not allow turbulent motions below to penetrate above. Nevertheless, the turbulent motions may erode the above layer so that the CBL increases its thickness by the entrainment of air from above.

The CBL is characterized by updrafts and downdrafts. The updraft is produced by the warm air, with low density; the downdraft, for the continuity mass equation, transports more slowly the cooled air, with high density, from top to bottom of the layer. In this way, the probability density function (pdf) of the vertical velocity w appears asymmetrical compared to a Gaussian pdf because of the stronger vertical motions of the updraft.

The height of the CBL depends on the heat fluxes at the ground and on the condition of the atmosphere above. At mid-latitude, for example, it reaches 1 or 2 Km by mid-afternoon in summer time because of the strong surface heating. The development of the CBL from sunrise consists in:

1. the heating causes the breakdown of the nocturnal inversion, and a shallow, mixed layer develops;

2. the shallow, mixed layer becomes a deep, well-mixed layer with a capping inversion called interfacial layer;

3. in the upper regions of CBL, a stable stratification is developed (related to entrainment processes across the inversion);

4. a surface inversion related to surface cooling develops prior the sunset.

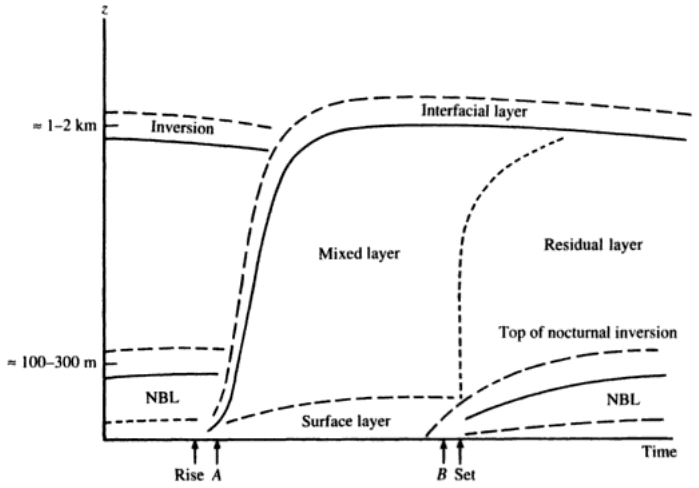

Figure 1.3: A schematic representation about the time evolution of CBL by mid-afternoon in summer time and at mid-latitude, taken from Garratt (1992)

It is possible to point out better the differences in the various layers in the CBL in the following way:

- the surface layer: where z is of the order of $|L_{MO}|$, according to the Monin-Obukov theory. Mean profiles, spectra and integral statistics depend upon $\zeta = \frac{z}{L_{MO}}$, except that for horizontal velocity turbulence components, for which $\frac{h}{L_{MO}}$ is the relevant scaling (where h is the CBL depth). Here the velocity scale is u_* and the temperature scale is θ_*;

- the free convection layer: it is confined to $|L_{MO}|<z<0.1h$. Here the velocity scale is w_* and the temperature scale is θ_{**}, defined as:

$$w_* = \left(\frac{g}{\theta_{00}} \overline{w'\theta'}|_0 z \right)^{\frac{1}{3}} \tag{1.18}$$

$$\theta_{**} = \frac{\overline{w'\theta'}|_0}{w_*} \tag{1.19}$$

and for this case the velocity and temperature profiles are given by:

$$\frac{d\overline{u}}{dz} \approx \frac{w_*}{z} = \left(\frac{g}{\theta_{00}}\overline{w'\theta'}|_0\right)^{\frac{1}{3}} z^{-\frac{2}{3}} \tag{1.20}$$

$$\frac{d\overline{\theta}}{dz} \approx -\frac{\theta_{**}}{z} = \left(\frac{g}{\theta_{00}}\right)^{-\frac{1}{3}} \left(\overline{w'\theta'}|_0\right)^{-\frac{2}{3}} z^{-\frac{4}{3}} \tag{1.21}$$

- the mixed layer: it is confined to $0.1h<z<h$, that comprises most of the CBL and which is characterized by large values of the turbulent velocity scale w_*;
- the inversion layer: it is dominated by local entrainment effects and by the properties of the capping inversion and stable region above. Its depth may be as much as $0.5h$.

Between the surface layer and the free convection layer,there is a transition layer according to Kader and Yaglom (1990). They called it *dynamical-convective layer*, because of the transition nature of itself. In this layer the buoyancy is important for the production of vertical velocity fluctuations, and the horizontal components are due to shear (so mechanical origins).

Chapter 2

Horizontal homogeneity and equations

2.1 The equations

2.1.1 RANS equations

In this work, the horizontal homogeneity approximation is considered. This means that the horizontal variation of all variables is set zero ($\frac{\partial}{\partial x} = \frac{\partial}{\partial y} = 0$). The Navier-Stokes equations with a Reynolds average (RANS) are taken as motion equations for fluids. A Reynolds average is an *ensamble average*, i.e. an average made on a large number of events of the same phenomenon. This kind of average is possible if the system can be defined as ergodic, then only if the considered system is stationary so that the average in time equals the ensamble average. Anyhow, in real cases, the stationarity is another considered approximation (in fact, just think of a diurnal cycle for the atmospheric case). All variables are taken as the sum of a mean term and a fluctuating term (the symbol $\overline{[\quad]}$ means the ensamble average computation). An example can be expressed through a generic variable ϕ:

$$\phi = \overline{\phi} + \phi' \tag{2.1}$$

with the properties $\overline{\phi} = \overline{\overline{\phi}} + \overline{\phi'}$ and $\overline{\phi'} = 0$.

In agreement to many books, the subscript 1, 2 or 3 in a variable, indicates its component along the x-axis, y-axis and z-axis respectively. For the velocity field, in particular, they coincide with u, v and w component of the velocity wind and both the notations will be used depending on which is the most convenient. The following equations are the original RANS equations, valid for the mean field of velocity wind:

$$\frac{D\overline{u}_i}{Dt} = -\frac{1}{\rho_{00}}\frac{\partial \overline{p}}{\partial x_i} + \varepsilon_{ij3} f \overline{u}_j + \nu \frac{\partial^2 \overline{u}_i}{\partial x_j \partial x_j} + \delta_{i3}\frac{g}{\theta_{00}}\overline{\theta} - \frac{\partial \overline{u_i' u_j'}}{\partial x_j} \tag{2.2}$$

where $\frac{D}{Dt} \equiv \frac{\partial}{\partial t} + \overline{u}_j \frac{\partial}{\partial x_j}$ is the material derivative, ρ_{00} is a constant density value taken as reference value, $\overline{p}$ is the mean pressure, f is the Coriolis parameter and $\overline{u_i' u_j'}$ represents the momentum flux related to the fluctuating part (linked to the Reynolds stress term). For the pressure term, the geostrophic balance relations can be used:

$$-\frac{1}{\rho_{00}}\frac{\partial \overline{p}}{\partial x} = -f v_g \tag{2.3}$$

$$-\frac{1}{\rho_{00}}\frac{\partial \overline{p}}{\partial y} = f u_g \tag{2.4}$$

For the horizontal homogeneity, the horizontal derivatives and the third component of the mean velocity wind $\overline{w}$ are set zero, due to the absence of convergence and divergence over a flat terrain.
The viscosity term can be neglected because of the turbulent motion considered: in fact, for high Reynolds number values, ν is not very important.
In this way, the final RANS equations for the wind velocity become:

$$\frac{\partial \overline{u}}{\partial t} = f\left(\overline{v} - v_g\right) - \frac{\partial \overline{u'w'}}{\partial z} \tag{2.5}$$

$$\frac{\partial \overline{v}}{\partial t} = -f\left(\overline{u} - u_g\right) - \frac{\partial \overline{v'w'}}{\partial z} \tag{2.6}$$

in which the continuity equation for incompressible fluids is used:

$$\frac{\partial u_i}{\partial x_i} = 0 \tag{2.7}$$

that can be written also as follows, due to Reynolds decomposition:

$$\frac{\partial \overline{u}_i}{\partial x_i} = 0 \qquad \frac{\partial u_i'}{\partial x_i} = 0 \tag{2.8}$$

Another variable, whose evolution is described through a Reynolds average, is the potential temperature θ:

$$\frac{D\overline{\theta}}{Dt} = \chi \frac{\partial^2 \overline{\theta}}{\partial x_j \partial x_j} + H - \frac{\partial \overline{u_j' \theta'}}{\partial x_j} \tag{2.9}$$

in which the last term represents the heat fluxes along x_j direction, χ is the thermal diffusivity and H contains any sources and sinks of heat. The eq. (2.9), under the approximations used already for the velocity vector, becomes:

$$\frac{\partial \overline{\theta}}{\partial t} = -\frac{\partial \overline{w'\theta'}}{\partial z} + H \tag{2.10}$$

2.2 Second order moments

The equations described before, for the mean fields, need a closure on the second order moments (SOMs), i.e. on the terms that contains the fluxes. In this Section various ways to make a closure will be discussed.

2.2.1 The flux-gradient relation

A way to close the equations (2.5), (2.6) and (2.10) is using the first order closure, i.e. the flux-gradient relation. Under all the considered approximations, the closures at the first order for the Reynolds stresses are, as it can be seen also in Section (1.2.3):

$$\overline{u'w'} = -K_m \frac{d\overline{u}}{dz} \tag{2.11}$$

$$\overline{v'w'} = -K_m \frac{d\overline{v}}{dz} \tag{2.12}$$

$$\overline{w'\theta'} = -K_h \frac{d\overline{\theta}}{dz} \tag{2.13}$$

where the diffusion coefficients follow the general formula:

$$K_m = l_m^2 2 \left(\overline{S_{ij} S_{ij}}\right)^{\frac{1}{2}} \tag{2.14}$$

$$K_h = K_m / Pr \tag{2.15}$$

and where $\overline{S_{ij}} = \frac{1}{2}\left(\frac{\partial \overline{u}_i}{\partial x_j} + \frac{\partial \overline{u}_j}{\partial x_i}\right)$ and Pr is the Prandtl number. The eq. (2.14) represents a general formulation for the diffusivity coefficient that, for the approximations here made, can not be used. Then, to compute the diffusivity coefficient, the eq. (1.15) is used. A classical parameterization for the mixing length l_m is taken from Blackadar (1962):

$$l_m{}^{-1} = (kz)^{-1} + l_0{}^{-1} \tag{2.16}$$

where l_0 has a fixed constant value. In this way, the size of the vortices (related to l_m) is limited over a certain height.

Anyhow, in the CBL, the use of the flux-gradient relation might not be a good solution to simulate the atmosphere. For this reason, a different approach was introduced by Deardorff (1966): he added a counter-gradient term to the original flux-gradient relation. In this way, fluxes of a generic scalar variable ϕ could be represented by the following formula:

$$\overline{\phi' w'} = -K\left(\frac{d\overline{\phi}}{dz} - \gamma\right) \tag{2.17}$$

that reads also

$$\overline{\phi' w'} = -K\frac{d\overline{\phi}}{dz} + \overline{\phi' w'}|_{NL} \tag{2.18}$$

in which $K\gamma = \overline{\phi' w'}|_{NL}$, so that the total fluxes can be considered as the sum of local and non-local fluxes.

A way to model the non-local term is using the idea of mass-flux, so that the eq. (2.18) assumes the following form:

$$\overline{\phi' w'} = -K\frac{d\overline{\phi}}{dz} + M\left(\phi_{up} - \overline{\phi}\right) \tag{2.19}$$

where K is the diffusivity coefficient, $M = a_{up}w_{up}$ is called mass flux, a_{up} is the fractional area of the ensamble of updrafts (indicated by the subscript "up"), w_{up} is the vertical velocity of updrafts, $\overline{\phi}$ is a mean value of the variable chosen and ϕ_{up} represents the quantity related to the updrafts of the considered variable. In literature, some references about the mass flux theory and its application are in Soares et al. (2004), Pergaud et al. (2009), Mironov and Ritter (2005), Gryanik and Hartmann (2002), Kershaw and Gregory (1997), Tiedtke (1989).

Other less simplified expressions for the non-local term are described in the following parameterizations.
In Deardorff (1972), the parameterizations used regarded the flux-gradient relation for the vertical heat flux. In particular, he proposed a formulation for the diffusivity coefficient K_h and for the counter gradient term. Then the eq. (2.18), applied to the variable θ, is:

$$\overline{\theta' w'} = -K_h \frac{d\overline{\theta}}{dz} + \overline{\theta' w'}|_{NL} \tag{2.20}$$

where, for Deardorff

$$K_h = \frac{l_m \overline{w'^2}}{c\sqrt{\frac{1}{2}q^2}} \tag{2.21}$$

$$\overline{\theta' w'}|_{NL} = \frac{g}{\theta_{00}} \frac{k\overline{\theta'^2}}{c} \frac{z}{\sqrt{\frac{1}{2}q^2}} \tag{2.22}$$

c is a constant, l_m follows the definition contained in the eq. (2.16) and $\frac{1}{2}q^2$ is the turbulent kinetic energy, whose evolution is described by eq. (2.43).

Later, another parameterization for the heat flux was introduced by Holtslag and Boville (1993), prescribed for very unstable condition. It consists in:

$$K_h = k w_t z \left(1 - \frac{z}{h}\right)^2 \tag{2.23}$$

$$\gamma = d \frac{\overline{w'\theta'}|_0}{w_* h} \tag{2.24}$$

where h is the height of the CBL, w_* and w_t are velocity scales given by

$$w_* = \left(\frac{g}{\theta_{00}} \overline{w'\theta'}|_0 h \right)^{\frac{1}{3}} \tag{2.25}$$

$$w_t = \frac{w_m}{Pr} \tag{2.26}$$

with

$$w_m \approx 0.85 w_* \tag{2.27}$$

and the coefficients used are taken from Troen and Mahrt (1986) and are experimental coefficients:

$$d \approx \frac{a}{(0.85)^2} \tag{2.28}$$

$$a = 7.2 \tag{2.29}$$

For unstable conditions $Pr = 1$, then the product $K_h \gamma$ can be written as the following non-local flux:

$$\overline{\theta' w'}|_{NL} = 8.47k \frac{z}{h} \left(1 - \frac{z}{h}\right)^2 \overline{w'\theta'}|_0 \tag{2.30}$$

where h is the inversion height of the potential temperature profile.

Other parameterizations were introduced also for the momentum fluxes, through a prescribed diffusivity coefficient K_m and the non local fluxes. In particular, in Frech and Mahrt (1995):

$$K_m = k w_t h \left(1 - \frac{z}{h}\right)^2 \tag{2.31}$$

$$\overline{u_i' w'}|_{NL} = -S_m u_* \left(w_* + u_*\right) \left(\frac{z}{h}\right) \left(1 - \frac{z}{h}\right)^2 \frac{u_{i(sh)}}{|\overrightarrow{v_{sh}}|} \tag{2.32}$$

where $S_m = 0.8$ is an empirical coefficient, $u_{i(sh)}$ is the i-th component of the bulk shear vector and w_t is a velocity scale defined as:

$$w_t = \left(u_*^3 + 1.5k w_*^3\right)^{\frac{1}{3}} \tag{2.33}$$

A further parameterization was made in Brown et al. (2008) for $\overline{u_i'w'}|_{NL}$:

$$\overline{u_i'w'}|_{NL} = -\frac{2.7w_*^3}{u_*^3 + 0.6w_*^3}\left(\frac{z'}{h'}\right)\left(1-\frac{z'}{h'}\right)^2 \overline{u_i'w'}|_0 \tag{2.34}$$

where $z' = z - 0.1h$, $h' = h - 0.1h$ and it is added to the local fluxes only in the range $0.1 \leq z/h \leq 1$ (whereas the other parameterizations are added in the range $0 \leq z/h \leq 1$). The quantity $\overline{u_i'w'}|_0$ represents the momentum fluxes at the ground and is parameterized with the following formula:

$$\overline{u_i'w'}|_0 = u_*^2 \frac{u_{i(sh)}}{|\overrightarrow{v_{sh}}|} \tag{2.35}$$

The following schemes are useful to have a complete vision of the different parameterization for the diffusion coefficients and the non-local fluxes. In particular, the diffusivity coefficients are already seen in the eq. (1.15) as the product of a velocity scale U and a length scale L. In the following table, it is possible to see the differences among the different diffusion coefficients, to characterize the form assumed by U and L and to distinguish the presence of a shape function (absent in Deardorff (1972)), whose role is to weigh the local vertical gradient of the quantity in question ($\overline{u}$, $\overline{v}$ or $\overline{\theta}$) depending on the level at which it is computed.

Authors	K (m^2/s)	L (m)	U (m/s)	Shape function
Deardorff (1972)	eq. (2.21)	l_m	$\frac{\overline{w'^2}}{c\sqrt{\frac{1}{2}q^2}}$	
Holtslag and Boville (1993)	eq. (2.23)	z	$w_t = \frac{w_m}{Pr}$	$k\left(1-\frac{z}{h}\right)^2$
Frech and Mahrt (1995)	eq. (2.31)	h	$w_t = (u_*^3 + 1.5kw_*^3)^{\frac{1}{3}}$	$k\left(1-\frac{z}{h}\right)^2$

The non-local fluxes can be also seen as a composition of different terms: a term that controls the magnitude of them (as a function of the velocity scales for the momentum fluxes), a term containing a shape function (absent in Deardorff (1972) again) with

the same role assumed for the diffusion coefficients, and a term that determines the direction of the flux in question through its dependence from a shear wind (absent in the heat flux parameterizations).

Authors	flux	Magnitude	Shape function	Direction
Deardorff (1972)	eq. (2.22)	$\frac{g}{\theta_{00}}\frac{k\overline{\theta'^2}}{c}\frac{z\sqrt{2}}{\sqrt{\overline{u'^2}+\overline{v'^2}+\overline{w'^2}}}$		
Holtslag and Boville (1993)	eq. (2.30)	$8.47k\overline{w'\theta'}\vert_0$	$\frac{z}{h}\left(1-\frac{z}{h}\right)^2$	
Frech and Mahrt (1995)	eq. (2.32)	$-S_m u_*\left(w_*+u_*\right)$	$\left(\frac{z}{h}\right)\left(1-\frac{z}{h}\right)^2$	$\frac{u_{i(sh)}}{\vert\overrightarrow{v_{sh}}\vert}$
Brown et al. (2008)	eq. (2.34)	$-\frac{2.7w_*^3}{u_*^3+0.6w_*^3}u_*^2$	$\left(\frac{z'}{h'}\right)\left(1-\frac{z'}{h'}\right)^2$	$\frac{u_{i(sh)}}{\vert\overrightarrow{v_{sh}}\vert}$

2.2.2 The evolution equations for SOMs

Another way to close the equations (2.5), (2.6) and (2.10) is using the evolution equations for the second order moments. For the second order moments of velocity, the general formulation of the equations is:

$$\begin{aligned}\frac{D\overline{u_i'u_k'}}{Dt} &= \left(-\overline{u_i'u_j'}\frac{\partial\overline{u}_k}{\partial x_j}-\overline{u_k'u_j'}\frac{\partial\overline{u}_i}{\partial x_j}\right)-\frac{\partial\overline{u_i'u_j'u_k'}}{\partial x_j}\\ &+f\left(\varepsilon_{kj3}\overline{u_i'u_j'}+\varepsilon_{ij3}\overline{u_k'u_j'}\right)+\frac{g}{\theta_{00}}\left(\delta_{k3}\overline{u_i'\theta'}+\delta_{i3}\overline{u_k'\theta'}\right)\\ &-\frac{1}{\rho_{00}}\left(\overline{u_k'\frac{\partial p'}{\partial x_i}}+\overline{u_i'\frac{\partial p'}{\partial x_k}}\right)+\nu\left(\overline{u_k'\frac{\partial^2 u_i'}{\partial x_j\partial x_j}}+\overline{u_i'\frac{\partial^2 u_k'}{\partial x_j\partial x_j}}\right)\end{aligned} \tag{2.36}$$

where, on the right side:

- the first term is called *shear production term* and represents the turbulence produced by shear related to the mean field (this quantity enhances the turbulence present in a flow);
- the second term represents the momentum transport due to turbulence;
- the third term is called *buoyancy term* and represents the production/dissipation of turbulence due to buoyancy;
- the fourth term incorporates the Earth rotation effect through the Coriolis parameter;
- the fifth term represents the correlation between the fluctuations of velocity and the gradient of pressure fluctuations;
- the sixth term is the molecular dissipation term.

This last term can be written in a different way, so that it is possible to make some observations:

$$\nu\left(\overline{u'_k\frac{\partial^2 u'_i}{\partial x_j\partial x_j}}+\overline{u'_i\frac{\partial^2 u'_k}{\partial x_j\partial x_j}}\right)=\nu\frac{\partial^2\overline{u'_iu'_k}}{\partial x_j\partial x_j}-2\nu\overline{\frac{\partial u'_i}{\partial x_j}\frac{\partial u'_k}{\partial x_j}} \tag{2.37}$$

The first term on the right side of the eq. (2.37), in fact, represents the molecular diffusion of the second order moments $\overline{u'_iu'_k}$, while the second term represents the correlation between the first order derivatives of the velocity fluctuations. If the small scale turbulence is considered homogeneous and isotropic, the off-diagonal terms are zero. Then, if the dissipation is dominated by small scale phenomena, the second term becomes:

$$2\nu\overline{\frac{\partial u'_i}{\partial x_j}\frac{\partial u'_k}{\partial x_j}}\equiv\varepsilon_{ik}\simeq\frac{2}{3}\delta_{ik}\varepsilon \tag{2.38}$$

where

$$\varepsilon=\nu\overline{\left(\frac{\partial u'_i}{\partial x_j}\right)^2} \tag{2.39}$$

has a positive value and, in eq. (2.37), represents the molecular dissipation for the trace of the tensor $\overline{u'_iu'_k}$.

The second and the fifth terms of the eq. (2.36) represent the so called third order moments (TOMs), which will be discussed in Section (2.3).

The other SOM evolution equations, necessary to close the equations (2.5), (2.6) and (2.10), are the heat flux equations and, therefore, the evolution equation of the temperature variance:

$$\begin{aligned}\frac{D\overline{u_i'\theta'}}{Dt} = &\left(-\overline{u_i'u_j'}\frac{\partial\overline{\theta}}{\partial x_j} - \overline{\theta'u_j'}\frac{\partial\overline{u}_i}{\partial x_j}\right) - \frac{\partial\overline{u_i'u_j'\theta'}}{\partial x_j} - \delta_{i3}\frac{g}{\theta_{00}}\overline{\theta'^2} \\ &-\frac{1}{\rho_{00}}\overline{\theta'\frac{\partial p'}{\partial x_i}} + \left(\overline{\nu\theta'\frac{\partial^2 u_i'}{\partial x_j\partial x_j}} + \overline{\chi u_i'\frac{\partial^2\theta'}{\partial x_j\partial x_j}}\right)\end{aligned} \tag{2.40}$$

$$\frac{1}{2}\frac{D\overline{\theta'^2}}{Dt} = -\overline{u_i'\theta}\frac{\partial\overline{\theta}}{\partial x_i} - \frac{1}{2}\frac{\partial\overline{u_i'\theta'}}{\partial x_i} + \overline{\chi\theta'\frac{\partial^2\theta'}{\partial x_i\partial x_i}} \tag{2.41}$$

where the thermal dissipation is

$$\varepsilon_\theta = \overline{\chi\left(\frac{\partial\theta'}{\partial x_j}\right)^2} \tag{2.42}$$

and it owes its origins to a development of the last term (similarly to ε in the evolution equations (2.36)).

2.2.3 The turbulent kinetic energy (TKE) equation

A particular second order closure is constituted by the equation of the turbulent kinetic energy $\frac{1}{2}q^2 = \frac{1}{2}\overline{u_i'u_i'} = \frac{1}{2}\overline{u'^2} + \frac{1}{2}\overline{v'^2} + \frac{1}{2}\overline{w'^2}$:

$$\begin{aligned}\frac{D}{Dt}\left(\frac{1}{2}q^2\right) = &-\overline{u_i'u_j'}\frac{\partial\overline{u}_i}{\partial x_j} - \frac{\partial}{\partial x_j}\left(\frac{\overline{p'u_j'}}{\rho_{00}} + \frac{1}{2}\overline{u_i'u_i'u_j'}\right) \\ &+\frac{g}{\theta_{00}}\overline{w'\theta'} + \frac{\nu}{2}\frac{\partial^2 q^2}{\partial x_j\partial x_j} - \varepsilon\end{aligned} \tag{2.43}$$

The eq. (2.43) represents the time evolution of the trace of the Reynolds stress tensor, i.e. of its isotropic component.

2.3 Closure at higher order moments

If the SOM evolution equations are chosen to close the RANS equations, because they contain third order moment (TOM) terms, a new closure on TOMs is to introduce. The pressure term present in the equations (2.36) and (2.40) can be parameterized like in Stull (1988)):

$$\frac{1}{\rho_{00}}\overline{p'\left(\frac{\partial u_i'}{\partial x_j}+\frac{\partial u_j'}{\partial x_i}\right)} = -\frac{q}{3l_1}\left(\overline{u_i'u_j'}-\frac{\delta_{ij}}{3}q^2\right)+Cq^2\left(\frac{\partial \overline{u}_i}{\partial x_j}+\frac{\partial \overline{u}_j}{\partial x_i}\right) \tag{2.44}$$

$$\frac{1}{\rho_{00}}\overline{p'\left(\frac{\partial \theta'}{\partial x_j}\right)} = -\frac{q}{3l_2}\left(\overline{\theta' u_j'}\right) \tag{2.45}$$

where C is a constant and $l_1, l_2 \propto l_m$.

The momentum transport terms of the eq. (2.36) and its equivalent in the equations (2.40) and (2.41) are parameterized as:

$$\overline{u_i'u_j'u_k'} = -q\lambda_1\left(\frac{\partial\overline{u_i'u_j'}}{\partial x_k}+\frac{\partial\overline{u_i'u_k'}}{\partial x_j}+\frac{\partial\overline{u_j'u_k'}}{\partial x_i}\right) \tag{2.46}$$

$$\overline{u_i'u_j'\theta'} = -q\lambda_2\left(\frac{\partial\overline{u_i'\theta'}}{\partial x_j}+\frac{\partial\overline{u_j'\theta'}}{\partial x_i}\right) \tag{2.47}$$

$$\overline{u_i'\theta'^2} = -q\lambda_3\frac{\partial\overline{\theta'^2}}{\partial x_i} \tag{2.48}$$

where $\lambda_1, \lambda_2, \lambda_3 \propto l_m$.

Anyhow, in this work second order moment closures based on the flux-gradient relation have been used. For detailed informations on the higher order closure, it is possible to see some applications in Canuto et al. (2007), Canuto et al. (1994) and Cheng et al. (2005).

2.4 Boundary layer height

The boundary layer height (also called mixing height (MH)) is an important parameter because of its influence on both the mean flow and the turbulent structure. There is not only one definition about this parameter since its determination is related

to the data avaible to different authors, and so to the way used by them to find it. Some definition can be, for example:

- from Beyrich (1997) (used by Seibert et al. (2000) and Pietroni et al. (2012)): "The mixing height is the height of the layer adjacent to the ground over which pollutants or any constituents emitted within this layer or entrained into it become vertically dispersed by convection or mechanical turbulence within a time scale of about an hour."

- from Stull (1988) (used by Caporaso et al. (2013)): "We can define the boundary layer as the part of the troposphere that is directly influenced by presence of the earth's surface, and responds to surface forcings with a timescale of about an hour or less. These forcings include frictional drag, evaporation and transpiration, heat transfer, pollutant emission, and terrain induced flow modification. The boundary layer thickness is quite variable in time and space, ranging from hundreds of meters to a few kilometers."

In the case of a CBL study, anyhow, it is better to call the CBL height as inversion height than boundary layer height. In fact, CBL height and SBL height must be distinguished to be treated in different way. Among different ways to determine the inversion height of the CBL, there are:

- the determination of the inversion height of the potential temperature profile (from which the parameter takes its name) through the computation of the slope of θ profile or through the computation of the height at which the bulk Richardson number exceeds a critical value: $Ri_b \geq Ri_c$ (see i.e. Pietroni et al. (2012), Seibert et al. (2000));

- the determination of the minimum of fluxes: momentum fluxes (not very reliable for a CBL) or heat fluxes (more indicated than the last ones);

- the determination of the height at which there is the major vertical gradient of particle concentration;

- the "parcel method", for which the height is the equilibrium level of a hypothetical rising parcel of air (representing a thermal), that follows the dry adiabatic starting at the surface, with a measured or expected temperature, up to its intersection with the temperature profile;

- the determination of the first relative maximum in the backscattered echo intensity above a layer of well-developed convective activity (sodar measurements are necessary to use this method).

Chapter 3

Numerical model

3.1 BOLAM

BOLAM is a mesoscale meteorological model, developed by the CNR at the late 80's and it is the only meteorological model fully made in Italy. This model is written using Fortran 90 and makes a numerical integration of the equations that describe the motions and the thermodynamics of the atmosphere. A Single Column Model (SCM) is implemented on BOLAM: the FakeBolam. It is a 1-dimensional model and it is the model used in this work.

3.1.1 The SCM

As vertical coordinate, a z-coordinate grid is used to initialize the model, whereas a σ-coordinate grid is introduced and used to integrate the equations for consistency with the BOLAM model. The hydrostatic equation is used to transform the variables from z-coordinates to σ-coordinates. The set of equations (2.5), (2.6) and (2.10) are integrated in space using a staggered grid: once they are known in an initial time, together with their boundary conditions, they are integrated with a finite difference scheme. The aim of the staggered grid is to simplify the computations with the use of a central scheme. The integration in time of prognostic equations is performed using

a splitted scheme, called *forward-backward*, in which, in the forward part, a forward Euler scheme is used to integrate the Coriolis terms and, in the backward part, a fully-implicit scheme is used to integrate the vertical diffusion.

The vertical discretization is composed by integer levels and semi-integer levels: the integer levels are NLEV and the averaged variables are defined in these levels; the semi-integer levels are NLEV+1 (the excess level is at the ground, see the fig. (3.1) for a representation of the vertical scheme) and $\dot{\sigma}$, TKE, mixing length, turbulent fluxes (plus other quantities not included in the integer levels) are defined here.

The imposed boundary conditions are: $\dot{\sigma} = 0$ at the top and at the bottom of the scheme, the fluxes are zero at the top, the no-slip condition is imposed at the bottom (then, $u = 0$ and $v = 0$, only at the NLEV+1 of semi-integer levels), the velocity wind equals the geostrophic wind velocity at the top, a skin temperature is forced at the bottom (at the NLEV+1 of the semi-integer levels) as a function of time.

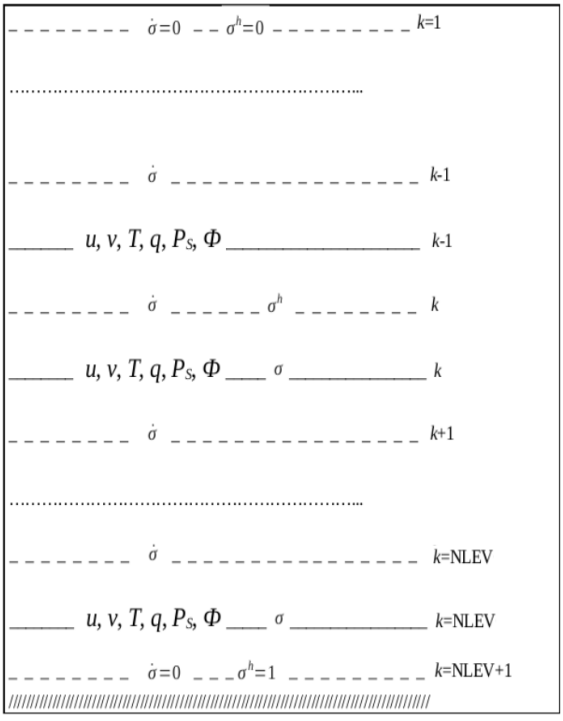

Figure 3.1: Discretization of the SCM vertical grid. The dashed lines are the semi-integer levels, whereas the full lines are the integer levels. The distance between two integer levels and between two semi-integer levels is given by the vertical resolution dz.

3.1.2 FakeBolam

The main program of the SCM is FakeBolam. It contains:

- the initialization of all the variables used (included in a subroutine called *fake_bolam_init*);
- the initial conditions of the wind speed, the potential temperature, the absolute temperature, the moisture, the TKE and the fluxes; the top condition of the wind speed and the computation of the absolute temperature, starting from a potential temperature profile and using its definition given by the eq. (1.1) (included in a subroutine called *condiniziali_init*);
- the definition of the grid in z-coordinate (through a subroutine called *griglia_init*);
- the transformation of the z-coordinate grid in a σ-coordinate grid (using a subroutine called *convertsigma_init*);
- the integration in time of the prognostic equations;
- the computation of integer and semi-integer levels of the geopotential;
- the calling to other subroutines described later: *coriolis*, *vdiff*, *tridiag*, *phicomp*, *temp_potenziale*;
- the computation of the mixing height, using alternative methods to that used by the original SCM (it has been included for this work);
- the writing output.

The subroutines *fake_bolam_init*, *condiniziali_init*, *griglia_init* and *convertsigma_init*, mentioned above, stay in a module called *mod_fake_bolam*, in which a forcing at the ground is also defined through the evolution in time of the absolute temperature (the so-called *tskin*).

In the subroutine *coriolis* there is the computation of the temporal evolution of the velocity components due to the Coriolis force.

In the subroutine *vdiff* the TKE-l closure is included. In particular this subroutine consists in:

- the surface layer parameterization;
- the computation of the mixing height as the level at which the potential temperature begins to increase;

- the numerical integration of the TKE;
- the computation of the diffusivity coefficients;
- the vertical diffusion of: the wind speed, the mixing ratio, the virtual potential temperature (computed using tskin), the TKE;
- the computation of heat and moisture fluxes at the ground.

In particular, the diffusion is computed also through the inversion of a tridiagonal matrix, included in the subroutine *tridiag*.

The subroutine *phicomp* contains the computation of the geopotential in the integer levels.

The subroutine *temp_potenziale* contains the computation of the potential temperature on integer and semi-integer levels.

In addition to subroutines, there are also some modules:

- *mod_bolam*: it contains SCM's parameters, constants and vectors;
- *mod_fake_bolam*: it contains the subroutines *fake_bolam_init*, *condiniziali_init*, *griglia_init*, *convertsigma_init* already described;
- *mod_mixing_lenght*: it computes a mobile average of the quantities required to calculate the mixing length l_m;
- *module*: useful to store the variables.

Finally, there are the following three files:

- *bolam.inp*: it contains the definition of the time-step and the duration in time of the run;
- *dimensions.inc*: it contains the total dimension of the SCM;
- *parametri.inp*: it contains the vertical resolution and the initial conditions of the program.

3.1.3 Surface layer parameterization in *vdiff*

It is expected that, between the lowest σ-level and the modeled terrestrial surface, a layer with constant fluxes is present and the Monin-Obukhov similarity theory is valid. In this way, if the atmospheric variables at the lowest level are known, it is possible to compute the surface fluxes.
From the integration of the equations (1.5) and (1.6) between the level $z = z_0$ (where z_0 is the height at which the lower boundary condition is applied and represents the roughness) and $z_0 < z = z_a < z_{NLEV}$. There are two possible schemes to use that depend on the stability of the atmosphere. If the atmosphere has an unstable stratification, the stability functions used by the model are the Businger functions (taken from Fleagle and Businger (1980)):

$$\psi_m(\zeta_0, \zeta_a) = \int_{\zeta_0}^{\zeta_a} \Phi_m(\zeta)\, d\zeta = \left[ln \left[\frac{\left(1 + (1-\gamma\zeta)^{\frac{1}{4}}\right)^2 \left(1 + (1-\gamma\zeta)^{\frac{1}{2}}\right)}{8} \right] - 2tan^{-1}(1-\gamma\zeta)^{\frac{1}{4}} + \frac{\pi}{2} \right]_{\zeta_0}^{\zeta_a} \tag{3.1}$$

$$\psi_h(\zeta_0, \zeta_a) = \int_{\zeta_0}^{\zeta_a} \Phi_h(\zeta)\, d\zeta = \left[2ln \left[\frac{\left(1 + (1-\gamma\zeta)^{\frac{1}{2}}\right)}{2} \right] \right]_{\zeta_0}^{\zeta_a} \tag{3.2}$$

where $\zeta_0 = \frac{z_0}{L_{MO}}$, $\zeta_a = \frac{z_a}{L_{MO}}$ and $\gamma = 16$.
In the case of stable stratification, the stability functions used are the Holtslag functions (taken from Beljaars and Holtslag (1991)):

$$\psi_m(\zeta_0, \zeta_a) = \int_{\zeta_0}^{\zeta_a} \Phi_m(\zeta)\, d\zeta = \left[- \left[a\zeta + b\left(\zeta - \frac{c}{d}\right) e^{-(d\zeta)} + \frac{bc}{d} \right] \right]_{\zeta_0}^{\zeta_a} \tag{3.3}$$

$$\psi_h(\zeta_0, \zeta_a) = \int_{\zeta_0}^{\zeta_a} \Phi_h(\zeta)\, d\zeta = \left[- \left[\left(1 + \frac{2}{3}a\zeta\right)^{\frac{3}{2}} + b\left(\zeta - \frac{c}{d}\right) e^{-(d\zeta)} + \frac{bc}{d} - 1 \right] \right]_{\zeta_0}^{\zeta_a} \tag{3.4}$$

where $a = 1$, $b = \frac{2}{3}$, $c = 5$ and $d = 0.35$.

In this way, it is possible to compute in the surface layer:

$$V(z_a) = \frac{u_*}{k}\left(ln\frac{z_a}{z_{0m}} - [\psi_m(\zeta_a) - \psi_m(\zeta_{0m})]\right) \tag{3.5}$$

$$\theta_v(z_a) - \theta_{vSKIN} = \frac{\theta_*}{k}\left(ln\frac{z_a}{z_{0T}} - [\psi_h(\zeta_a) - \psi_h(\zeta_{0T})]\right) \tag{3.6}$$

$$q(z_a) - q_S = \frac{q_*}{k}\left(ln\frac{z_a}{z_{0q}} - [\psi_h(\zeta_a) - \psi_h(\zeta_{0q})]\right) \tag{3.7}$$

where $\zeta_{0m} = \frac{z_{0m}}{L_{MO}}$, $\zeta_{0T} = \frac{z_{0T}}{L_{MO}}$ and $\zeta_{0q} = \frac{z_{0q}}{L_{MO}}$, and where z_{0m}, z_{0T} and z_{0q} are, respectively, the roughness for wind, for temperature and for mixing ratio.
The term $\frac{z_a}{L_{MO}}$ is iteratively solved using the following equation:

$$\frac{z_a}{L_{MO}} = Ri_b\frac{\left(ln\frac{z_a}{z_{0m}} - [\psi_m(\zeta_a) - \psi_m(\zeta_{0m})]\right)^2}{\left(ln\frac{z_a}{z_{0T}} - [\psi_h(\zeta_a) - \psi_h(\zeta_{0T})]\right)} \tag{3.8}$$

where $z_a = \frac{\Phi_{NLEV} - \Phi_{ground}}{g} + z_{0m}$ and the bulk Richardson number is defined as:

$$Ri_b = \frac{g z_a(\theta_{vNLEV} - \theta_{vSKIN})}{\overline{\theta} V_{NLEV}^2} \tag{3.9}$$

Once computed $\frac{z_a}{L_{MO}}$, the velocity scale u_*, the temperature scale θ_* and the surface fluxes for the sensible heat and for the mixing ratio are computed:

$$u_* = \frac{k\sqrt{u_{NLEV}^2 + v_{NLEV}^2}}{ln\left(\frac{z_a}{z_{0m}}\right) - \psi_m(\zeta_{0m}, \zeta_a)} \tag{3.10}$$

$$\theta_* = \frac{k(\theta_{vNLEV} - \theta_{vSKIN})}{ln\left(\frac{z_a}{z_{0T}}\right) - \psi_h(\zeta_{0T}, \zeta_a)} \tag{3.11}$$

$$\Phi_H = \frac{\rho_S C_{DT}(\theta_{vSKIN} - \theta_{vNLEV})}{\left(\frac{p_0}{p_S}\right)^{\frac{R_d}{c_p}}\left(1 + \left(\frac{1}{\varepsilon} - 1\right) q_{SKIN}\right)} c_{pd} \tag{3.12}$$

$$\Phi_q = \rho_S C_{Dq}(q_{SKIN} - q_{NLEV}) \tag{3.13}$$

where c_{pd} is the specific heat of the dry air taken with constant pressure, ε is the ratio

between the mass of vapour and the total mass of air, and the coefficients C_{DT} and C_{Dq} are given by:

$$C_{DT} = \frac{ku_*}{\left(ln\frac{z_a}{z_{0T}} - [\psi_h(\zeta_a) - \psi_h(\zeta_{0T})]\right)} \tag{3.14}$$

$$C_{Dq} = \frac{ku_*}{\left(ln\frac{z_a}{z_{0q}} - [\psi_h(\zeta_a) - \psi_h(\zeta_{0q})]\right)} \tag{3.15}$$

3.1.4 The TKE-l closure

In the SCM, the evolution equations considered for the turbulent diffusion of both momentum and potential temperature are:

$$\frac{\partial \overline{u}_i}{\partial t} = -\frac{1}{\rho}\frac{\partial\left(\rho\overline{w'u_i'}\right)}{\partial z} \tag{3.16}$$

$$\frac{\partial \overline{\theta}}{\partial t} = -\frac{1}{\rho}\frac{\partial\left(\rho\overline{w'\theta}\right)}{\partial z} \tag{3.17}$$

that are the equations (2.5) and (2.6) without the Coriolis term and the eq. (2.10) without the sources/sinks term (both these terms are calculated separately).

The closure used in the original SCM for the second order moments is a TKE-l closure, in which the TKE equation, applying the SCM simplification, is:

$$\frac{\partial}{\partial t}\left(\frac{1}{2}q^2\right) = -\frac{\partial}{\partial z}\left(\frac{\overline{p'w'}}{\rho_{00}} + \frac{1}{2}\overline{u_i'u_i'w'}\right) - \overline{u_i'w'}\frac{\partial \overline{u}_i}{\partial z} + \frac{g}{\theta_{00}}\overline{w'\theta'} - \varepsilon \tag{3.18}$$

where the turbulent fluxes of momentum are:

$$\overline{u'w'} = -K_m\frac{\partial \overline{u}}{\partial z} \tag{3.19}$$

$$\overline{v'w'} = -K_m\frac{\partial \overline{v}}{\partial z} \tag{3.20}$$

such as the equations (2.11) and (2.12), and the heat flux recall the eq. (2.13):

$$\overline{\theta'u_j'} = -K_h\frac{\partial \overline{\theta}}{\partial x_j} \tag{3.21}$$

In these closures, the diffusion coefficients used are dependent on the mixing length and are parameterized as follows:

$$K_m = l_m \sqrt{c_e \left(\frac{1}{2} q^2\right)} \tag{3.22}$$

$$K_h = \frac{K_m}{Pr} \tag{3.23}$$

where $c_e = 0.17$ and the Prandtl number is computed depending on the stability of the simulated atmosphere:

$$Pr = \begin{cases} 1 + 5.0\, Ri & \text{per } Ri \geq 0 \quad (3.24) \\ 1 & \text{per } Ri < 0 \quad (3.25) \end{cases}$$

In the eq. (3.22), K_m is calculated using the expression given by the eq. (1.15): l_m is the length scale and the velocity scale is proportional to the square root of the TKE. The computation of the mixing length l_m depends on the stability too: for the stable case, a modified Blackadar mixing length is used (see Blackadar (1962))

$$l_m = \frac{kz l_{max}}{kz + l_{max}} \frac{1}{1 + 12Ri} \tag{3.26}$$

where l_{max} is the maximum value attributable to the mixing length and Ri is computed as the gradient Richardson number:

$$Ri = Ri_g = \frac{\frac{g}{\theta_{00}} \frac{\partial \overline{\theta}}{\partial z}}{\left(\frac{\partial \overline{u}}{\partial z}\right)^2 + \left(\frac{\partial \overline{v}}{\partial z}\right)^2} \tag{3.27}$$

For the unstable case, a non local parameterization is used, by modifying a formula proposed by Bougeault and Lacarrere (1989):

$$l_m = C_u \left[(h - z)\,(z - z_{down})^3\right]^{\frac{1}{4}} \tag{3.28}$$

where $C_u = 0.5$, h is the top of the unstable layer computed as the first level, starting from the ground, at which the term $\frac{dlog\theta}{dz}$ is positive, z_{down} is taken as the height at the lowest level (NLEV+1) and it must be $z_{down} < z < h$.

The third order moments term, present in the TKE equation, describes the vertical diffusion of the TKE. For this reason, in analogy to the momentum and the heat fluxes, this term is modeled with the following flux-gradient relation:

$$\frac{\partial}{\partial z}\left(\frac{\overline{p'w'}}{\rho_{00}}+\frac{1}{2}\overline{u_i'u_i'w'}\right)=\frac{\partial}{\partial z}\left[-K_m\frac{\partial}{\partial z}\left(\frac{1}{2}q^2\right)\right] \tag{3.29}$$

using the inversion of a tridiagonal matrix.

The dissipation term ε is computed through:

$$\varepsilon=\frac{\sqrt{c_e\left(\frac{1}{2}q^2\right)^3}}{l_m} \tag{3.30}$$

In this way, the prognostic TKE equation for the original SCM is:

$$\frac{\partial}{\partial t}\left(\frac{1}{2}q^2\right)=\frac{\partial}{\partial z}K_m\frac{\partial}{\partial z}\left(\frac{1}{2}q^2\right)+K_m\left(\frac{\partial\overline{u}}{\partial z}\right)^2+K_m\left(\frac{\partial\overline{v}}{\partial z}\right)^2-K_h\frac{g}{\theta_{00}}\frac{\partial\overline{\theta}}{\partial z}-\frac{\sqrt{c_e\left(\frac{1}{2}q^2\right)^3}}{l_m} \tag{3.31}$$

The fig. (3.2) shows how the TKE-l closure works. This scheme is applied for all grid point and at every iteration time.

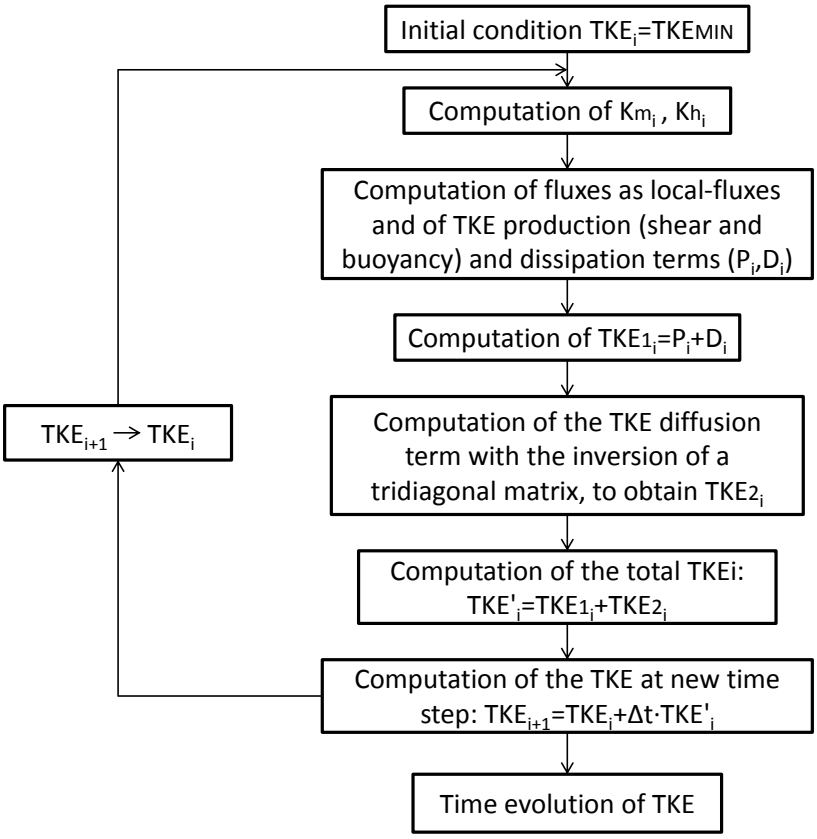

Figure 3.2: A schematic representation of the steps followed by the SCM for the computation of TKE and fluxes.

3.2 The modified TKE-l closure

In Section (2.2.1) other ways useful to close the evolution equations have been described for the CBL. They use a modified flux-gradient relation expressed by the general eq. (2.18), in which a non-local term is added to the local fluxes. For this work, the non-local fluxes added to the equations (3.19), (3.20) and (3.21) are those prescribed in Holtslag and Boville (1993) (eq. (2.30)), Frech and Mahrt (1995) (eq. (2.32)) and Brown et al. (2008) (eq. (2.34)).

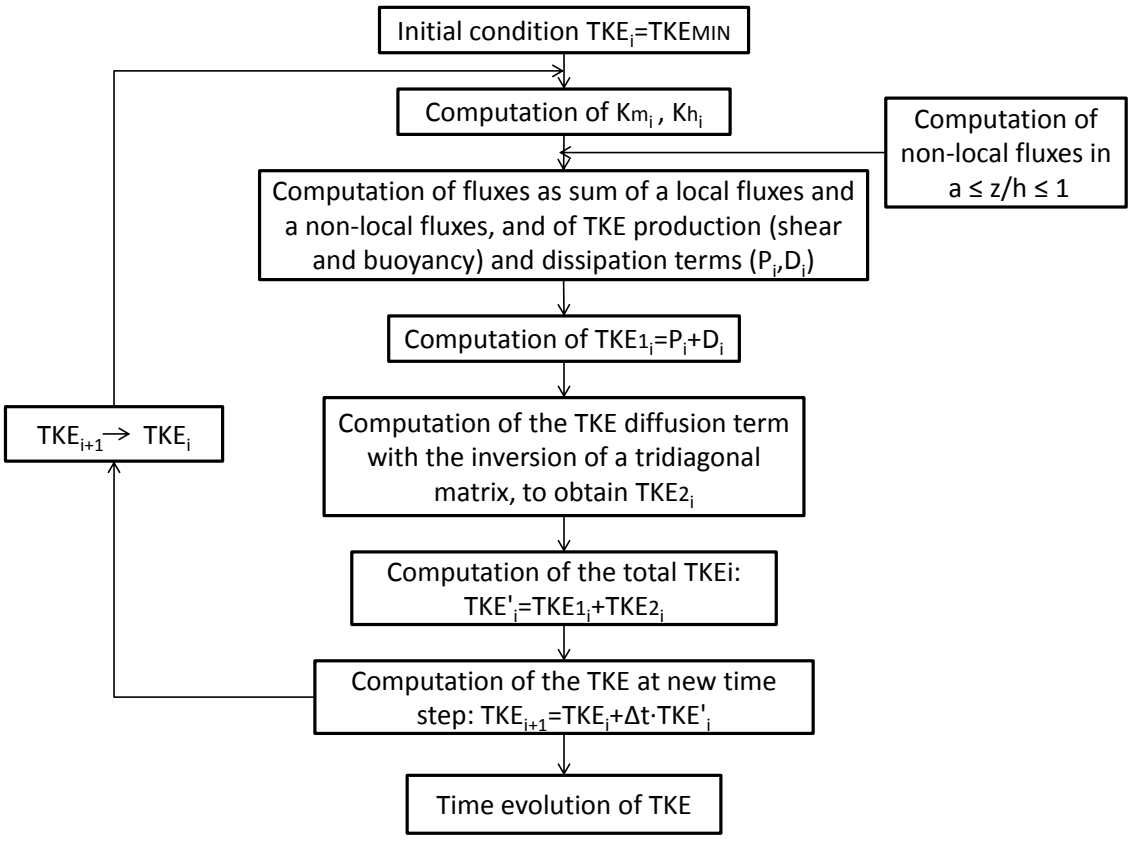

Figure 3.3: A schematic representation of the steps followed by the SCM for the computation of TKE and fluxes with the introduction of the non-local parameterizations.

In the program used, this changes are done in the subroutine called *vdiff*: inside the TKE-l closure loop there is a calling to a new subroutine (that can be *holtslag*, *frechmahrt* or *brown*) that add the non-local term of fluxes to the local one only in the mixed layer, in a range $a \leq z/h \leq 1$ (where a depends on the closure used and it can be $a = 0$ or $a = 0.1$ for the considered cases).

In fig. (3.3) a scheme of the modified TKE-l loop is represented.

3.3 MH determination

In the SCM model, the height of the CBL is determined in the subroutine *vdiff*, as it is already said. It consists in placing the height equal to the lowest level near the ground, when the heat flux at the ground is negative, and equal to the first level,

starting from the ground, at which the term $\frac{dlog\theta}{dz}$ is positive, when the heat flux at the ground is positive.

Other ways to determine the MH have been introduced in FakeBolam, so that a comparison is possible to do. In particular, two methods has been included:

- the determination of the mixing height through the computation of the level at which the gradient Richardson number exceeds a critical value: $Ri_g \geq Ri_c = 0.3$ (see Seibert et al. (2000)), where Ri_g is computed using the eq. (A.2);
- the determination of the height at which there is an absolute minimum of the heat fluxes, using the function MINLOC(): it returns the level at which there is the minimum value of the heat flux.

Chapter 4

Numerical results

4.1 The GABLS2 experiment

To simulate a CBL in the SCM, i.e. a diurnal evolution cycle, the GABLS2 experiment is considered (see Svensson et al. (2011)). The acronym GABLS stay for GEWEX Atmospheric Boundary Layer Study, where GEWEX, in turn, stay for Global Energy and Water cycle EXperiment. The number that follows it indicates that it is the second experiment made within the GABLS.

GABLS2 is based on observations taken during the Cooperative Atmosphere-Surface Exchange Study-1999 (Cases-99), held in Kansas (USA) in the early autumn with a strong diurnal cycle without clouds. In particular, the period begins at 1600 LT 22 October and continues for 59 hours. In the original and modified SCM, the initial and the boundary conditions used are based on the GABLS2 experiment: a geostrophic wind is imposed at the top of the simulated layer:

$$\begin{aligned} \overline{u}\,(z) &= u_g = 3m/s \\ \overline{v}\,(z) &= v_g = -9m/s \end{aligned} \tag{4.1}$$

and a skin temperature as a function of time (i.e. the temperature at the surface) is imposed as follows (fig. (4.1)):

$$
\begin{aligned}
T &= -10 - 25cos\,(0.22t + 0.2) && t \leq 17.4 \\
T &= -0.54t + 15.2 && 17.4 < t \leq 30 \\
T &= -7 - 25cos\,(0.21t + 1.8) && 30 < t \leq 41.9 \\
T &= -0.37t + 18.0 && 41.9 < t \leq 53.3 \\
T &= -4 - 25cos\,(0.22t + 2.5) && 53.3 < t \leq 65.5 \\
T &= 4.4 && t > 65.5
\end{aligned}
$$

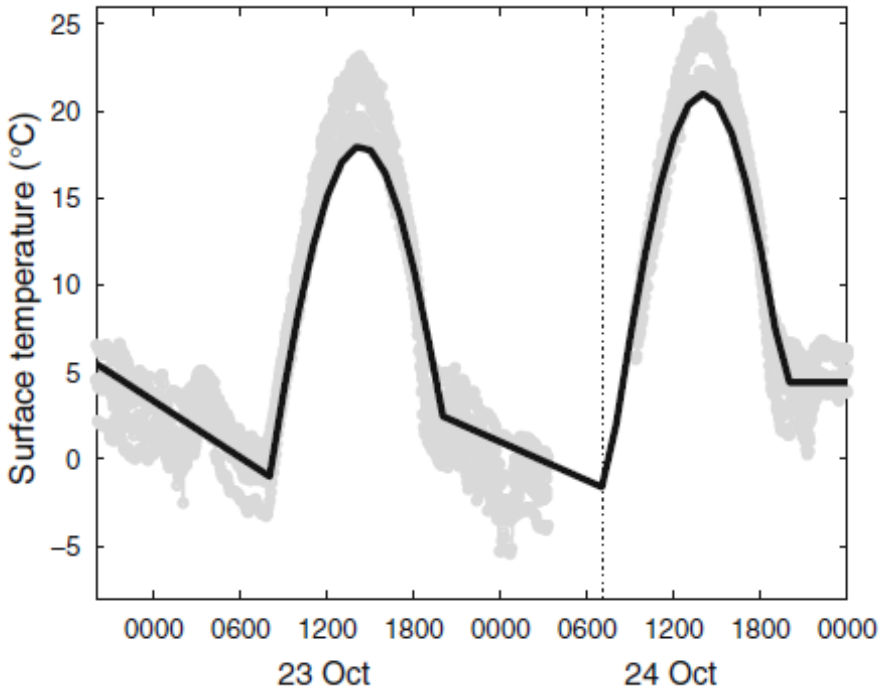

Figure 4.1: Surface temperature (°C) as a function of time. The observations are marked in gray and the fits from the simulations are in black.

Furthermore, an initial vertical profile of the potential temperature θ is imposed:

$\Theta(K)$	$z(m)$
288	0
286	200
286	850
288	900
292	1000
300	2000
310	3500
312	4000

4.2 Closures comparison

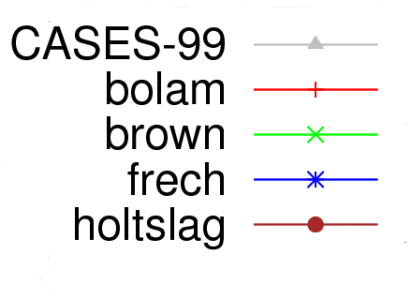

Figure 4.2: Illustration of the legend used in the following figures.

In this Section a comparison among the observations, the original SCM and the modified SCM is made. The vertical resolution dz used for the integration in space of the equations is set at 20m. For a better understanding, the legend is represented in fig. (4.2) and the symbology means:

- CASES-99: observations data;
- bolam: the original SCM closure is used;
- brown: the original SCM closure is modified by adding a non local term to the momentum fluxes, taken from Brown et al. (2008);
- frech: the original SCM closure is modified by adding a non local term to the momentum fluxes, taken from Frech and Mahrt (1995);

- holtslag: the original SCM closure is modified by adding a non local term to the heat flux, taken from Holtslag and Boville (1993).

4.2.1 2-m temperature

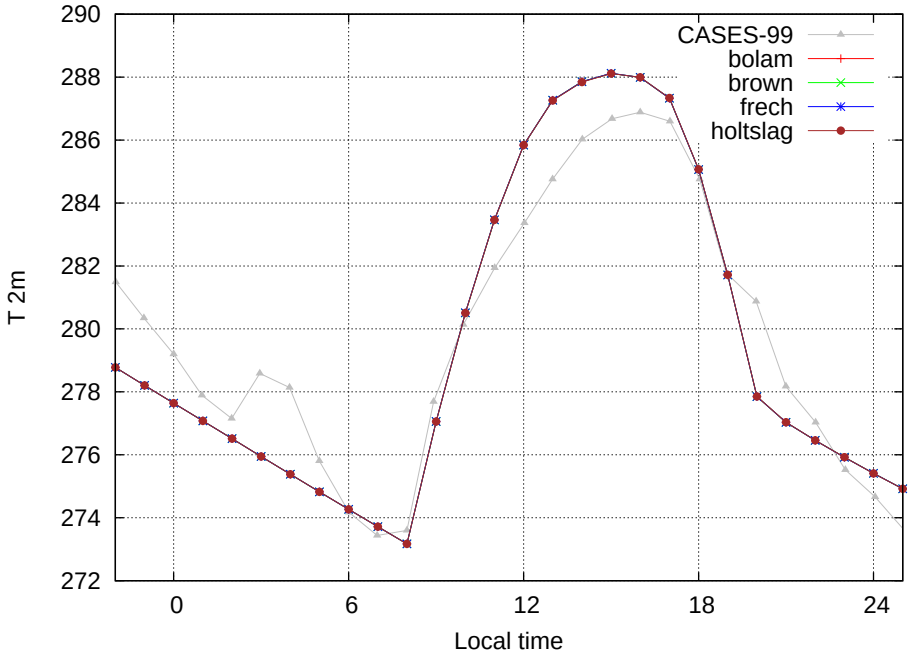

Figure 4.3: Time series of observed and simulated temperature (K) at 2 m a.g.l. since 2200 LT 22 October, for 27 hours.

In fig. (4.3), the observed and simulated 2-m temperature are shown. Observed data show a sudden increase in the temperature at about 0300 LT 23 October, due to a local disturbance (as it is declared in Svensson et al. (2011)). However, this phenomenon is not expected in the simulations since it is not included in the surface forcing.

The transition from night to day obtained by the simulations looks in accord to the observations and it is due to the prescribed surface temperature. In the first hour of the heating, the simulations show an increase of about $4K$, similar to the observations.

Before 0800 LT (i.e. before the heating of the surface) and after 1900 LT (i.e. during the cooling of the surface), the simulated temperature does not fit well the observed one. This result is due to the prescribed surface temperature: in fact, the fitted function is in the center of the observational range during nighttime and at its lower end during daytime.

During the diurnal evolution, the simulated 2-m temperature is warmer than the observed one and it is due to its dependence on the prescribed skin temperature, as it is possible to see from the following modified eq. (3.6):

$$\theta_v\left(z_0+2m\right)=\theta_{vSKIN}+\frac{\theta_*}{k}\left(ln\frac{z_0+2m}{z_{0T}}-\left[\psi_h\left(\frac{z_0+2m}{L_{MO}}\right)-\psi_h\left(\zeta_{0T}\right)\right]\right) \tag{4.2}$$

Furthermore, as it is possible to see in the next sections, the overestimate is due also to the diffusion contribution: in fact, the variable θ_* is computed as a function of θ_{NLEV} (eq. (3.11)).

4.2.2 Averaged TKE over the lowest $55m$ of the atmosphere

In fig. (4.4) the observed and simulated TKE are shown. The values illustrated are an average over the first $55m$ from the ground. During the night and during the warmest hours of the day, all the models overestimate slightly the value of the observations and it means that the simulated atmosphere is more diffusive then the observed one, although the heat flux at the ground doesn't reach high values (fig. (4.5)). In the first hours of the day, when the heating begins, all simulations underestimate the observations: this is due to the prescribed skin temperature.

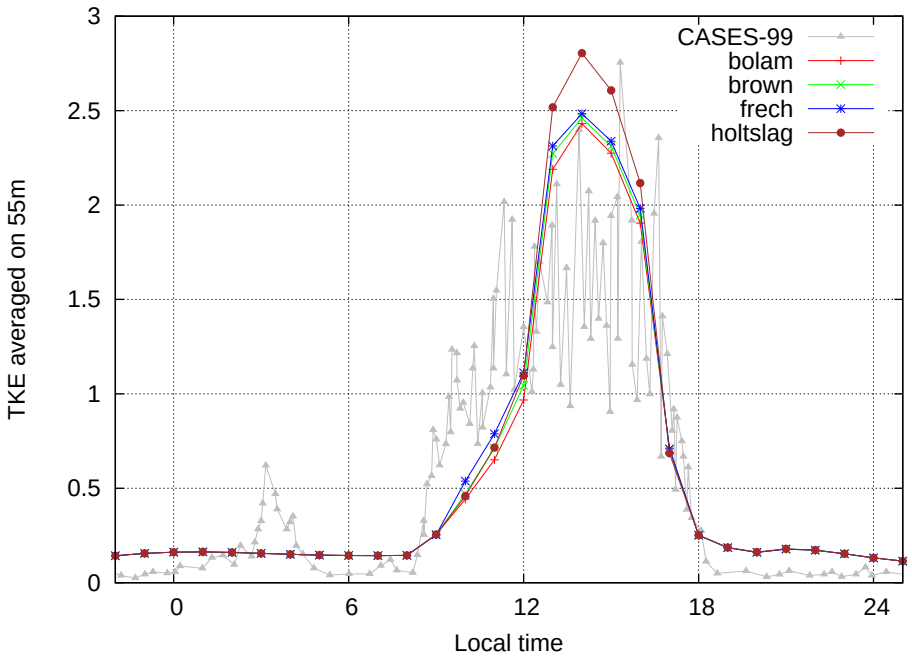

Figure 4.4: Time series of observed and simulated TKE (m^2/s^2) since 2200 LT 22 October, for 27 hours.

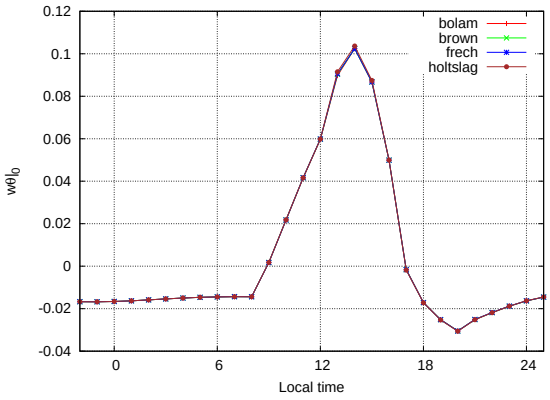

Figure 4.5: Time series of the simulated heat flux at the ground (Km/s) since 2200 LT 22 October, for 27 hours.

It is possible to see how the different closures used give only a small contribution to the computation of the TKE: the biggest differences are during the warmest hours of the day and the *holtslag* closure (for the heat flux) gives the highest values in that hours, as it possible to see in fig. (4.7), where the vertical profile of the TKE, the mixing length, the diffusivity coefficients, the momentum and heat fluxes and the shear and buoyancy terms are plotted at 1400LT 23 October (the warmest hour). Furthermore, it is possible to see that the shear term is only little affected by the modified momentum fluxes closures. From a comparison between fig. (4.6) and fig. (4.7) it is possible to observe how much the mixing length, the diffusivity coefficients, and then all the other variables that depend on them, increase during the warming hours. In fig. (4.6), in particular, it is possible to see that the unstable layer is still not well developed and it is near the ground.

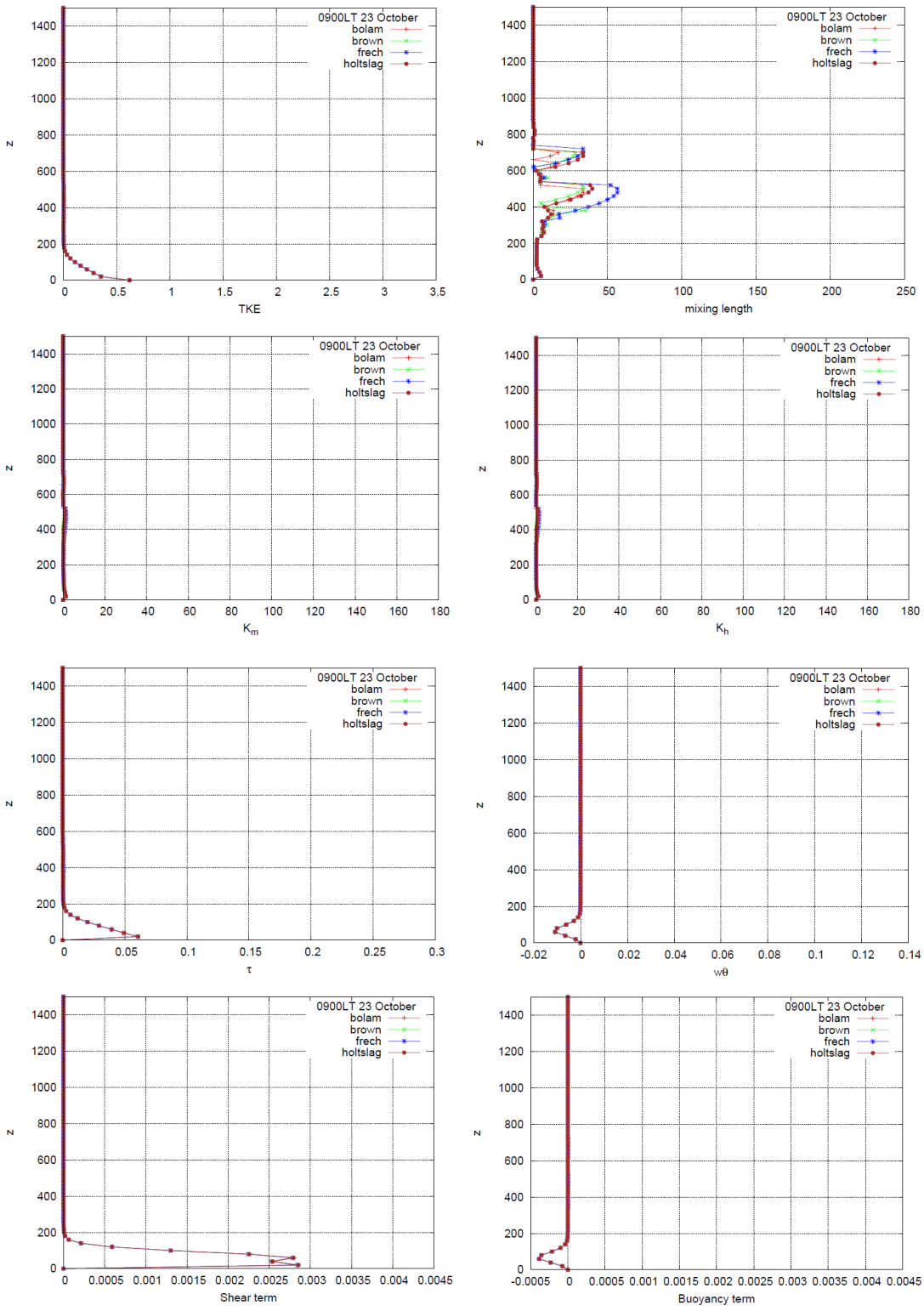

Figure 4.6: Vertical profile up to 1500m at 0900 LT 23 October of: TKE, mixing length, diffusivity coefficients, momentum and heat fluxes, shear and buoyancy terms.

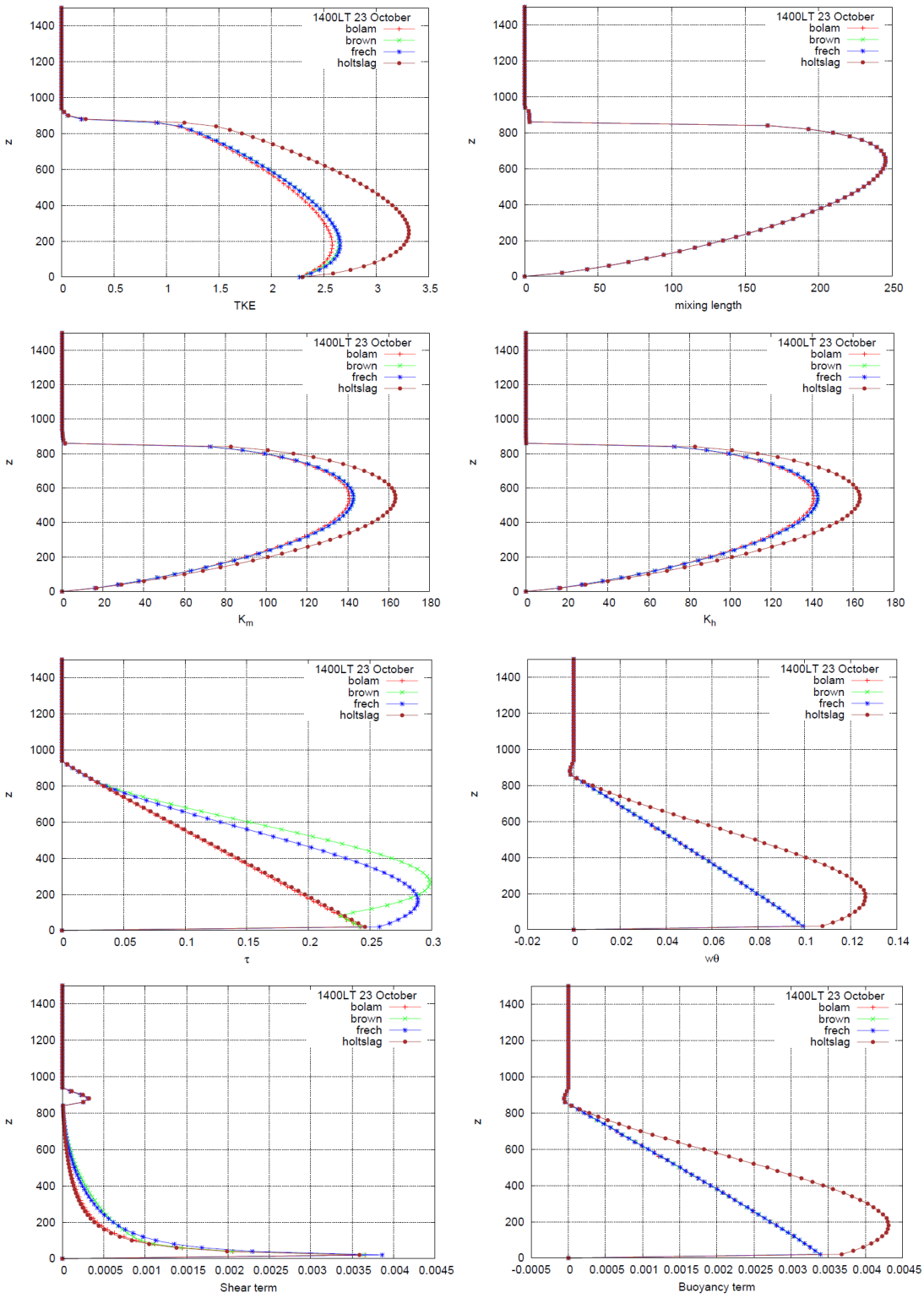

Figure 4.7: Vertical profile up to 1500m at 1400 LT 23 October of: TKE, mixing length, diffusivity coefficients, momentum and heat fluxes, shear and buoyancy terms.

4.2.3 Friction velocity and 10-m wind speed

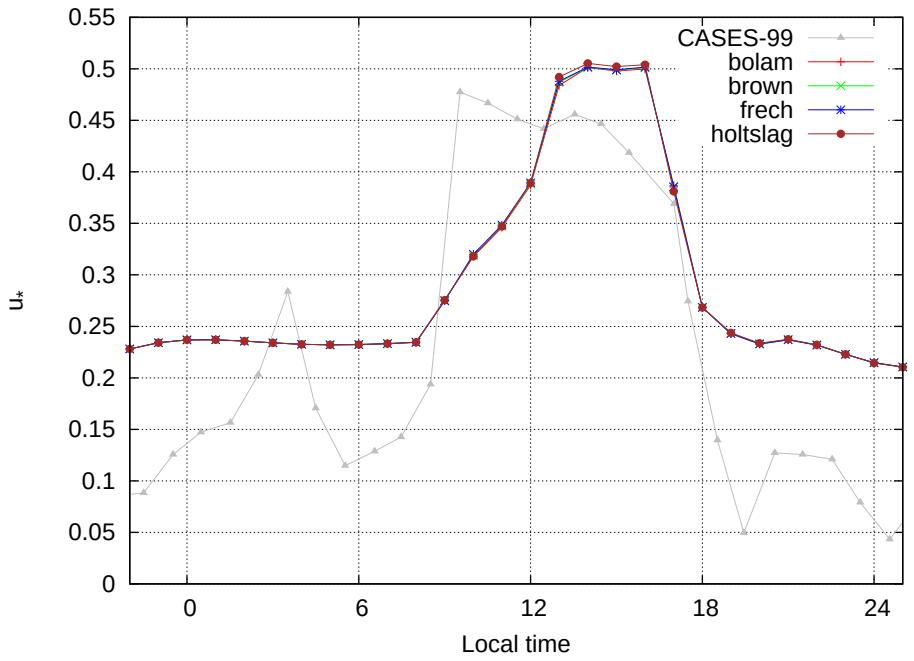

Figure 4.8: Time series of observed and simulated friction velocity u_* (m/s) since 2200 LT 22 October, for 27 hours.

In fig. (4.8) the observed and simulated friction velocity u_* are shown.

At about 0200 LT 23 October there is a peak related to the same local disturbance seen in fig. (4.3) and omitted in the surface temperature forcing.

It is possible to note that, even if the transition from night to day is visible and follows the trend of the prescribed temperature at the surface, all the simulations overestimate the value assumed by the friction velocity. Since it is computed using the eq. (3.10) and the quantity $|V_{NLEV}|$ is computed in the mixed layer, the overestimation can be explained with the high value assumed by $|V_{NLEV}|$ (fig. (4.9)), due to the diffusion contribution (also seen in fig. (4.4)).

In fig. (4.10) the observed and simulated 10-m wind speed are shown.

All the simulations show the same trend, due to the dependence of 10-m wind speed from the friction velocity (eq. (4.3)), and then it overestimate the observations too:

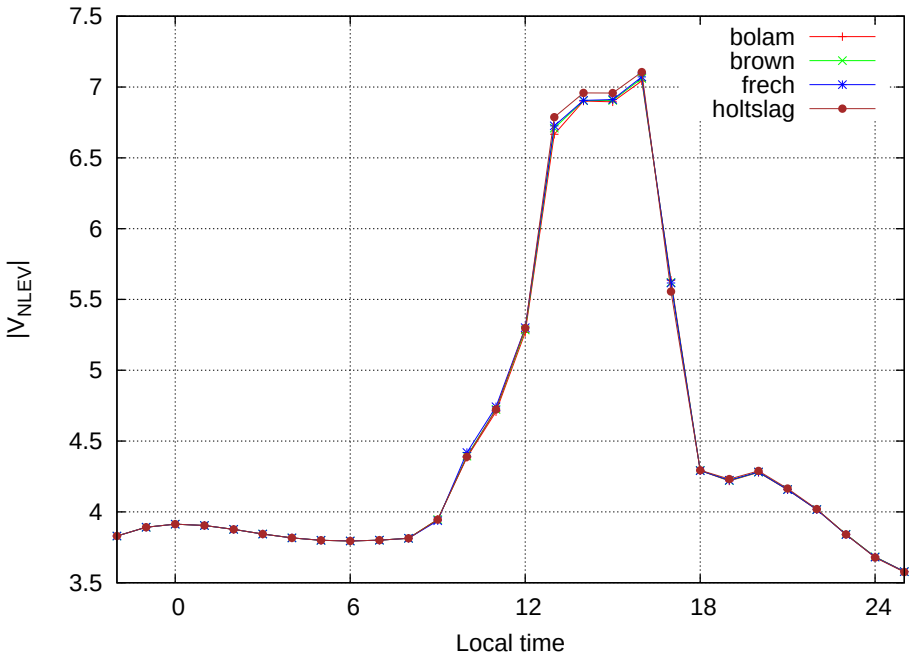

Figure 4.9: Time series of the simulated module of velocity at NLEV level (m/s) since 2200 LT 22 October, for 27 hours.

$$V\left(z_0+10m\right)=\frac{u_*}{k}\left(ln\frac{z_0+10m}{z_{0m}}-\left[\psi_m\left(\frac{z_0+10m}{L_{MO}}\right)-\psi_m\left(\zeta_{0m}\right)\right]\right) \tag{4.3}$$

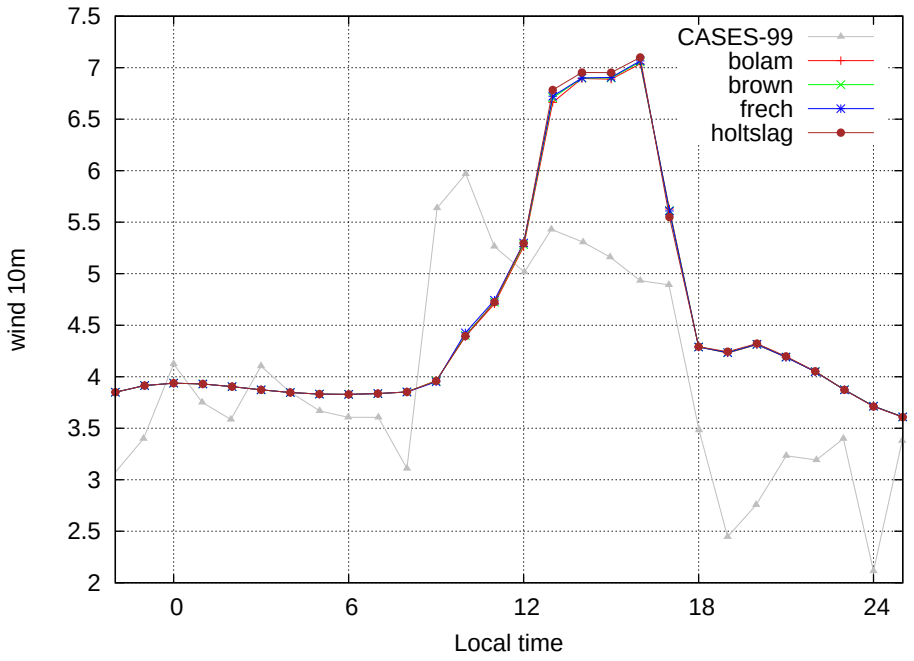

Figure 4.10: Time series of observed and simulated wind speed (m/s) at 10 m a.g.l. since 2200 LT 22 October, for 27 hours.

4.2.4 Mixing Height

In fig. (4.11) the observed and simulated mixing height are shown. A single value of the observations is present, at 1400 LT 23 October, and is about $850m$.

All the simulations reach, with the same trend, the value of the mixing height given by the observations.

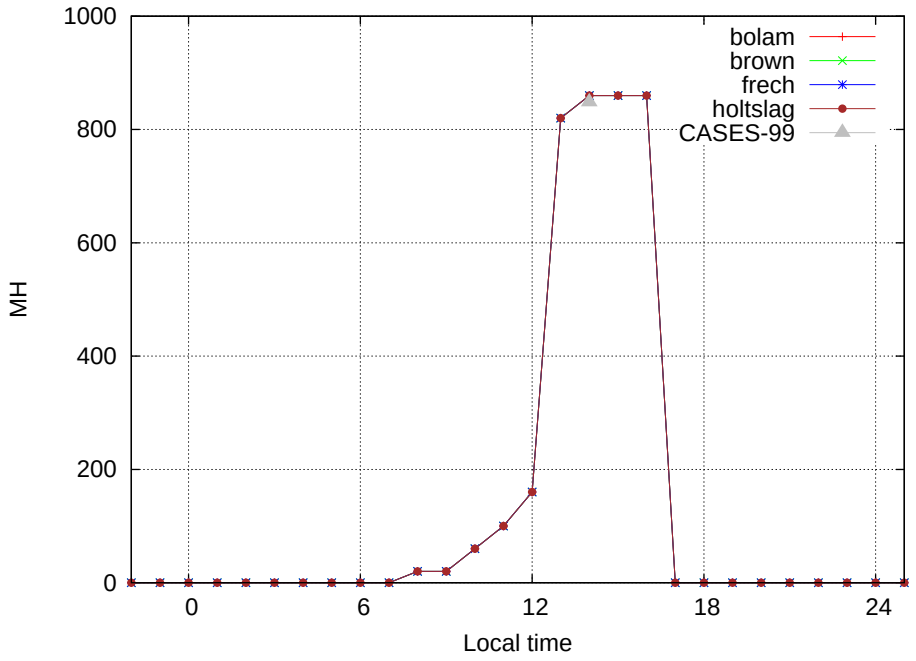

Figure 4.11: Time series of observed and simulated mixing height (m) since 2200 LT 22 October, for 27 hours. The value of the MH from CASES-99 is only at 1400 LT 23 October.

4.2.5 Potential temperature vertical profile

In fig. (4.12) the observed and simulated potential temperature θ vertical profiles are shown. All the simulations have the same trend, even though the different closures gives different TKE, and so different diffusivity coefficients. It is due to the overestimation of mixing, leading to a tendency of the model to produce a quasi-neutral profile of the temperature.

The capping inversion is reaches by all the simulations at the same height of that observed.

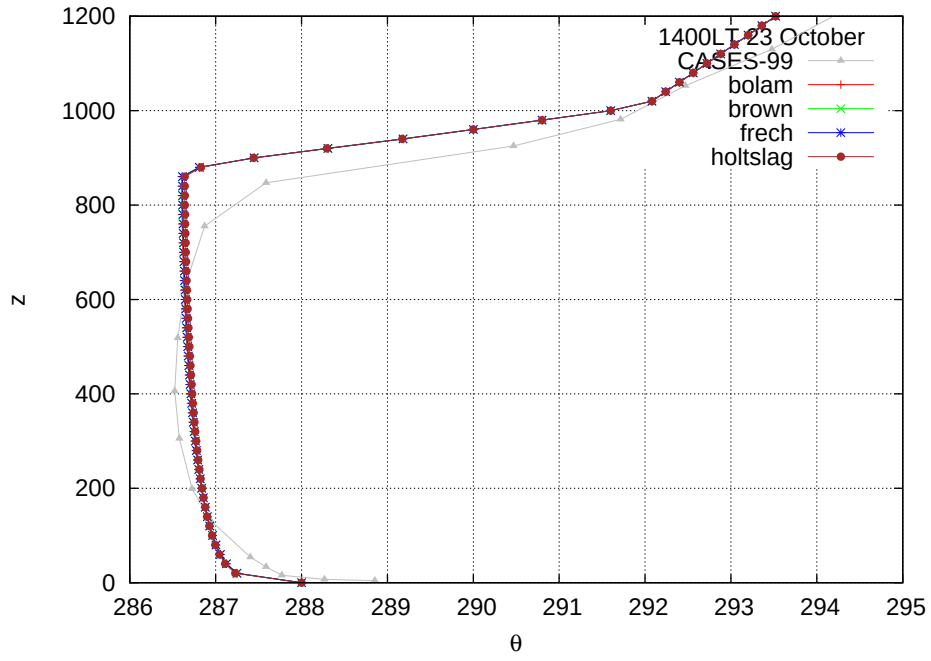

Figure 4.12: A vertical profile of the potential temperature θ (K) taken from observations and models at 1400 LT 23 October.

4.3 Comparison among different MH computations

In fig. (4.13), the mixing height is computed as the height at which there is the minimum value of the heat flux. The observed value is at the height $850m$, whereas the simulated one is at $900m$.

In fig. (4.14), the mixing height is computed as the height at which the gradient Richardson number reaches the critical value 0.3. The observed value is in agreement with the observed one.

In fig. (4.15), a comparison among the different methods used to compute the MH is represented. Since all the used closures have a similar trend considering each method, only the original SCM results are plotted. The mixing height computed through the potential temperature inversion and through the critical value of the gradient Richardson number reach the same value of the observations at 1400 LT 23 October, whereas the mixing height computed through the minimum value of the heat flux overestimates

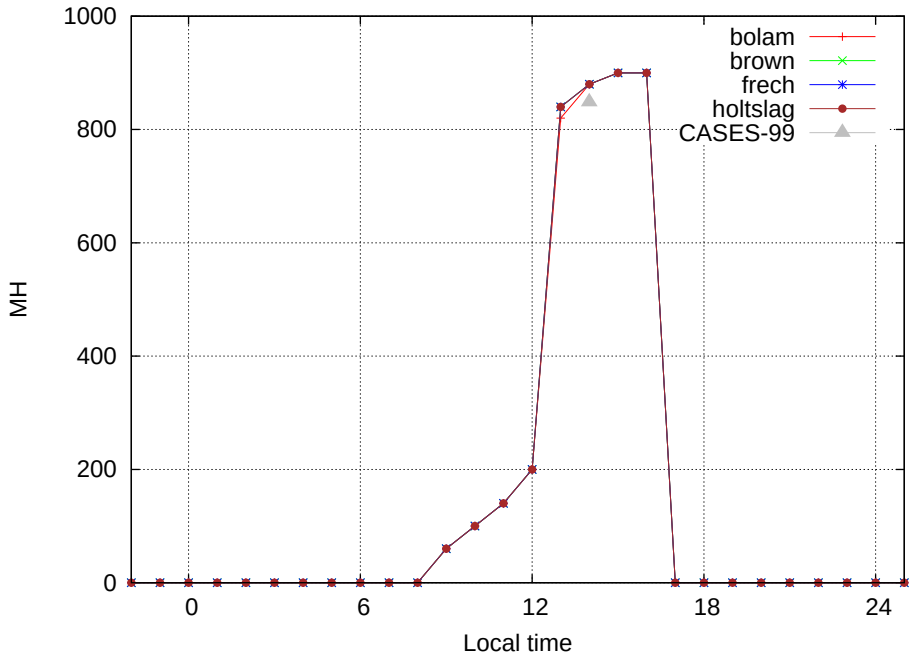

Figure 4.13: Time series of observed and simulated mixing height (m) computed through the minimum value assumed by the heat flux at every time step, since 2200 LT 22 October, for 27 hours. The value of the MH from CASES-99 is only at 1400 LT 23 October.

the observed value.

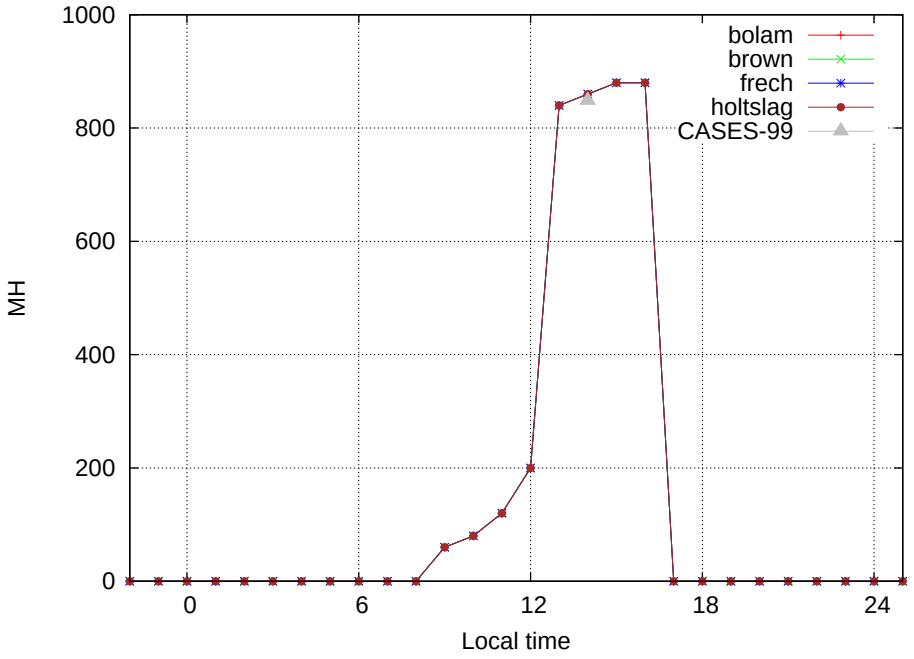

Figure 4.14: Time series of observed and simulated mixing height (m) computed through a critical value of the gradient Richardson number, since 2200 LT 22 October, for 27 hours. The value of the MH from CASES-99 is only at 1400 LT 23 October.

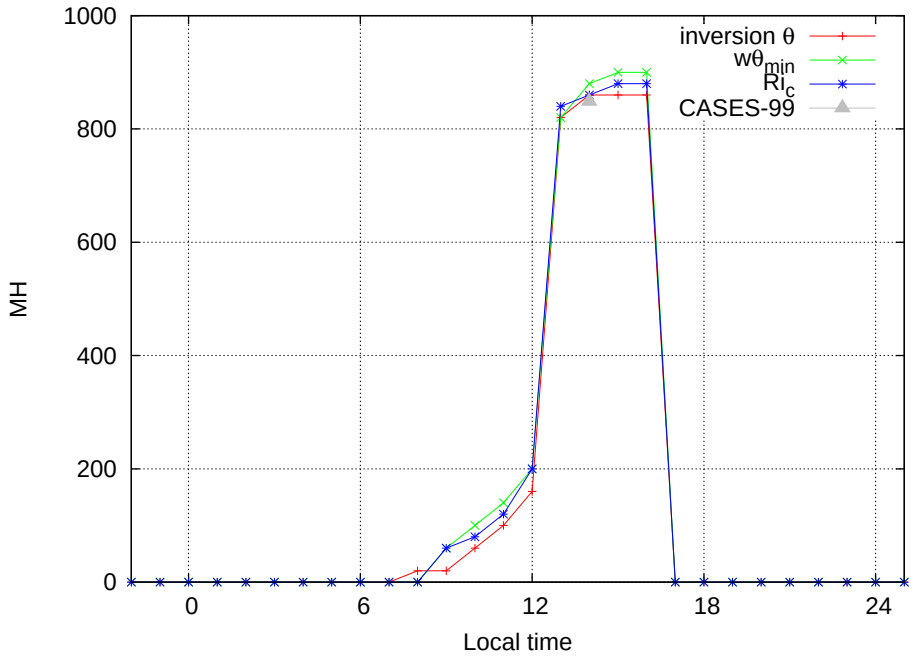

Figure 4.15: Comparison among the different methods used to compute the mixing height (m). The observed value of the MH from CASES-99 is only at 1400 LT 23 October. The time series start at 2200 LT 22 October and continue for 27 hours. In this figure only the not modified SCM is represented.

Conclusions

In this work a Convective Boundary Layer (CBL) has been simulated by a numerical model. For this aim, a Single Column Model (SCM) called FakeBolam is been used, suited to boundary layer studies and, in particular, to test different closures of the RANS equations.

The closure used by the original SCM is the BOLAM TKE-l (a second order closure), in which the fluxes are parameterized with the flux-gradient relation. Since the flux-gradient relations are not fully satisfactory to simulate a CBL, they have been modified adding a non-local term. Three different schemes are tested in this way, besides the original BOLAM scheme, in which the non-local fluxes are taken by Holtslag and Boville (1993) (for the heat flux), Frech and Mahrt (1995) and Brown et al. (2008) (these last two for the momentum fluxes).

The GABLS2 experiment has been used as a benchmark, the simulations are based on GABLS2-setup (initial and boundary conditions) and the results obtained by the four different schemes are compared with the observation provided by the study case. The three modified schemes give higher values of all the variables than the original SCM, as it is expected. In particular, the closure prescribed for the heat flux gives the highest values during the warmest hours: it produces a more diffusive regime than the other parameterizations as expected since in a CBL the buoyancy term, included in the TKE equation, plays an important rule.

On the other hand, since the original SCM overestimates the quantities in comparison with the observations (such as the TKE averaged on 55m from the ground, the friction velocity, the potential temperature at 2m from the ground and the wind speed at 10m from the ground), also the modified schemes overestimate them. This means that all the schemes simulate a more diffusive atmosphere than that observed in the case GABLS2.

Furthermore, among the different schemes used, the differences are little and it is due to the overestimation of the mixing leading to a tendency of the model to produce a quasi-neutral profile of the temperature.

In the formulation of the so-called local closure in BOLAM, the definition of the mixing length accounts for the boundary layer depth, thus some indirect non-local effects are taken into account. This means that the use of non-local formulations should be coupled with a proper modification of the original scheme (for instance, by making the mixing length formulation more local).

Appendices

Appendix A

The Richardson number

A.1 The flux, gradient and bulk Richardson numbers

In the introduction to the ABL, a distinction among the boundary layers was made through the sign of the vertical heat flux $\overline{w'\theta'}|_0$. Another possibility to distinguish the boundary layers is referring to them through the *flux Richardson number* Ri_f, defined as:

$$Ri_f = \frac{\frac{g}{\theta_{00}}\overline{w'\theta'}}{\overline{u'w'}\frac{\partial \overline{u}}{\partial z} + \overline{v'w'}\frac{\partial \overline{v}}{\partial z}} \tag{A.1}$$

where g is a mean value of the gravity acceleration, θ_{00} is a fixed value of the potential temperature at the ground, u and v are the zonal and the meridional component of the wind velocity respectively, $\overline{u'w'}$ and $\overline{v'w'}$ are the vertical momentum fluxes, and $\overline{w'\theta'}$ represents the vertical heat flux.
Then, the distinction among the boundary layers depends on the sign of Ri_f as follows:

- SBL if Ri_f>0;
- CBL if Ri_f<0;
- NBL if $Ri_f = 0$.

It is possible, using the flux-gradient relations (described in Section (1.2.3)), to find another Richardson number, called *gradient Richardson number* Ri_g, defined as:

$$Ri_g = \frac{\frac{g}{\theta_{00}}\frac{\partial\overline{\theta}}{\partial z}}{\left(\frac{\partial\overline{u}}{\partial z}\right)^2 + \left(\frac{\partial\overline{v}}{\partial z}\right)^2} \tag{A.2}$$

The two Richardson number just defined are proportional to each other through the *Prandtl number* Pr:

$$Ri_f = \frac{Ri_g}{Pr} \tag{A.3}$$

In the reality, anyhow, it is difficult to measure continue variables, then a *bulk Richardson number* Ri_b is defined:

$$Ri_b = \frac{g}{\theta}\frac{(\theta - \theta_0)z}{(u^2 + v^2)} \tag{A.4}$$

where variables are discretized.

A.2 The Richardson number in the TKE equation

The TKE equation (2.43), neglecting the molecular viscosity, becomes:

$$-\overline{u_i'w'}\frac{d\overline{u}_i}{dz} + \frac{g}{\theta_{00}}\overline{w'\theta'} - \frac{d}{dz}\left(\frac{\overline{p'w}}{\rho_{00}} + \frac{1}{2}\overline{u_i'u_i'w'}\right) - \varepsilon \simeq 0 \tag{A.5}$$

Using the definition of the flux Richardson number (A.1), the equation (A.5) can be written as:

$$-\overline{u_i'w'}\frac{d\overline{u}_i}{dz}(1 - Ri_f) - \frac{dT}{dz} - \varepsilon \simeq 0 \tag{A.6}$$

where T contains the third order moments. For the CBL will be Ri_f<0, for the NBL $Ri_f = 0$ and for the SBL Ri_f>0 (because of the heat flux that provide energy to the turbulence or not). For Ri_f>1 the production of turbulence, due to sheared motion, doesn't balance the dissipation term (if the divergence of third order terms is neglected), and a dissipation of turbulence is expected, together with the existence of a critical value of the Richardson number beyond which there is a very stable stratified situation. Anyhow, over this value, turbulence is present yet (usually intermittent turbulence), and it can be powered by the third order term flux.

A.3 Change of vertical resolution

An other experiment done using the SCM consists in changing the vertical resolution dz of the model: the simulations of the original SCM were made with dz=10m (NLEV=400), dz=20m (NLEV=200) and dz=50m (NLEV=80).

A general behavior is visible: the values of the variables at high resolution are higher than at low resolution. It can be seen, for example, in figures (A.1)-(A.2)-(A.3)-(A.4)-(A.5).

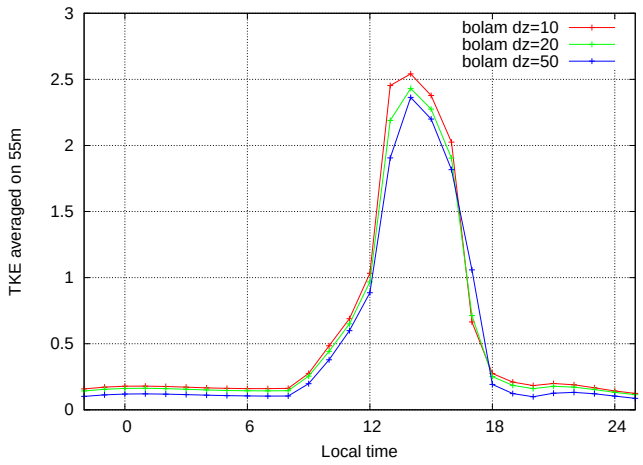

Figure A.1: Time series of simulated TKE (m^2/s^2) with different vertical resolutions, since 2200 LT 22 October, for 27 hours.

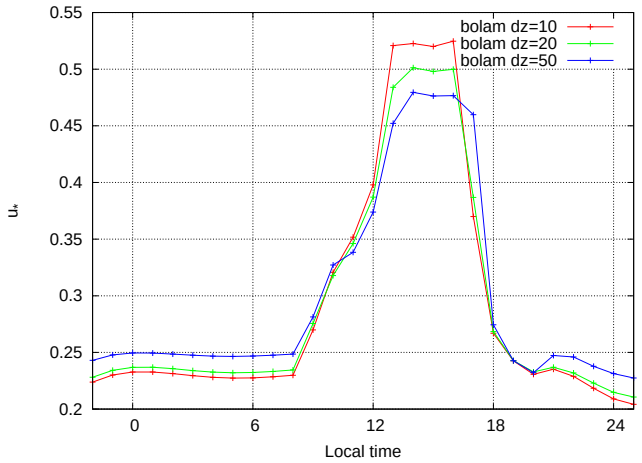

Figure A.2: Time series of simulated u_* (m/s) with different vertical resolutions, since 2200 LT 22 October, for 27 hours.

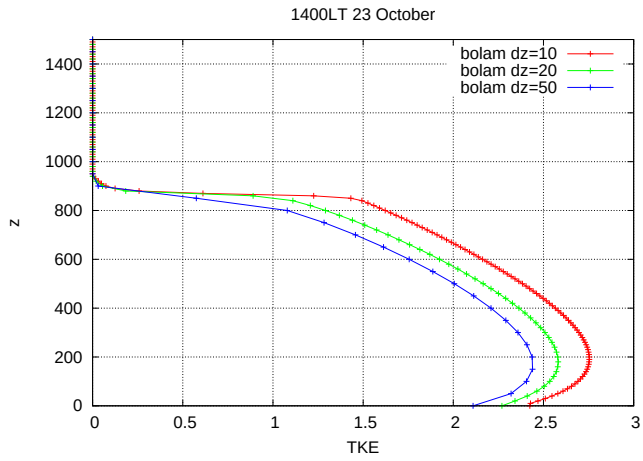

Figure A.3: Vertical profile of simulated TKE (m^2/s^2) with different vertical resolutions, at 1400 LT 23 October.

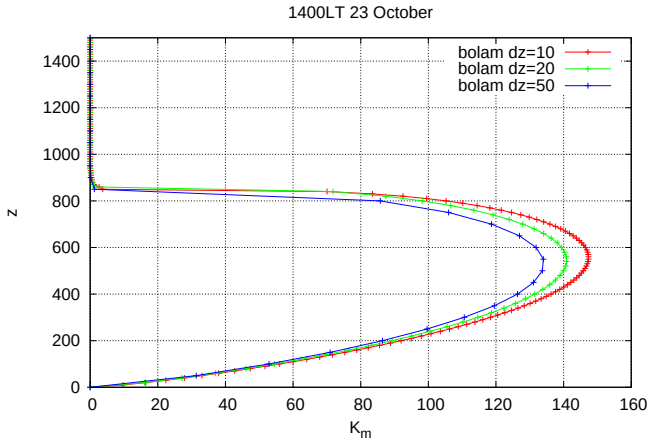

Figure A.4: Vertical profile of simulated diffusivity coefficient K_m (m^2/s) with different vertical resolutions, at 1400 LT 23 October

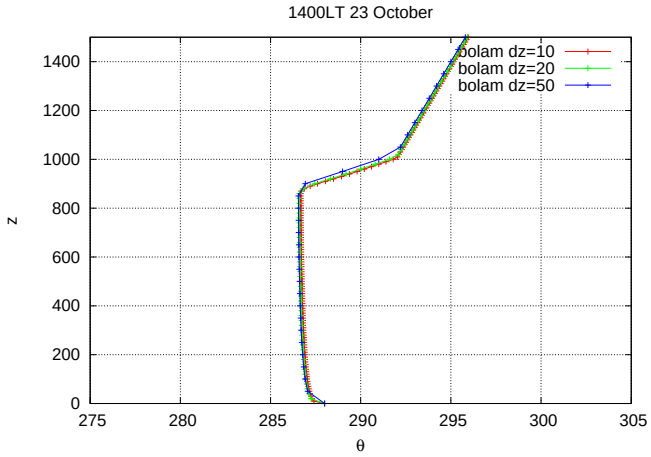

Figure A.5: Vertical profile of simulated θ (K) with different vertical resolutions, at 1400 LT 23 October.

In particular, in fig. (A.2), there is a different behavior between night and day: only

during the daytime the values reached by the highest resolutions are higher than the lowest ones. This is due to the stability function ψ_m, represented in fig.(A.6).

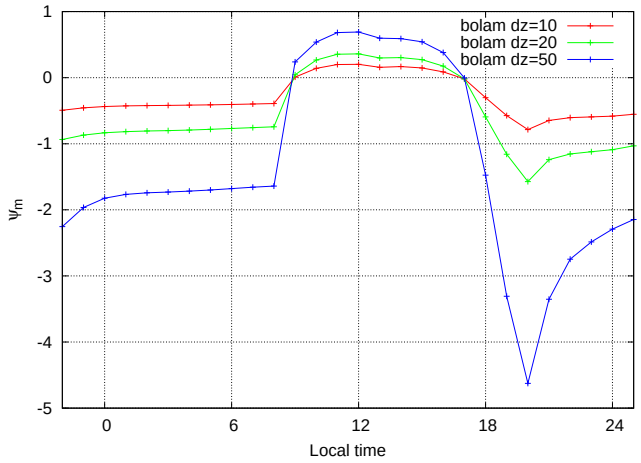

Figure A.6: Time series of simulated stability function ψ_m with different vertical resolutions, since 2200 LT 22 October, for 27 hours.

A particular result is obtained in the fig.(A.7), in which the wind speed at 10m from the ground is plotted: with the resolutions dz=50m and dz=20m its trend is due to its dependence from u_*, but, in the case in which dz=10m, the plot is not as it is expected. This is because, using the vertical resolution dz=10m, the wind speed at 10m from the ground is not computed through the similarity parameterization (as, instead, it is for the other resolutions used).

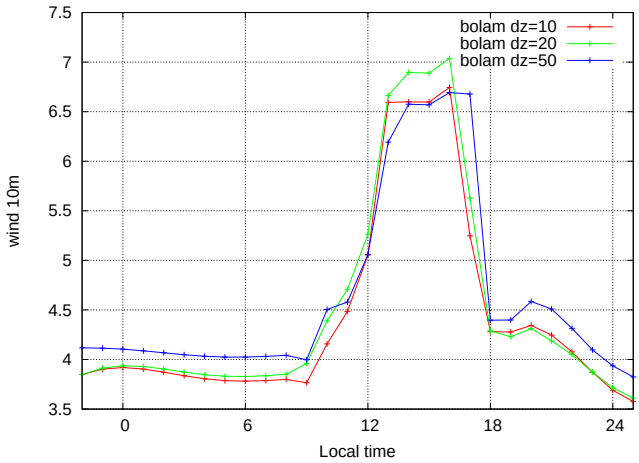

Figure A.7: Time series of simulated wind speed (m/s) at 10 m a.g.l. with different vertical resolutions, since 2200 LT 22 October, for 27 hours.

In fig.(A.8) the simulated mixing height with the different vertical resolutions are plotted. This is computed with the original method of the SCM: it is the height at which there is the inversion of θ. Since the CBL is simulated using the same initial and boundary conditions used for the main experiment (Section (4.1)), it is interesting to see that at 1400 LT the MH reaches about 850m, such as in the experiment GABLS2, even though the different vertical resolutions used.

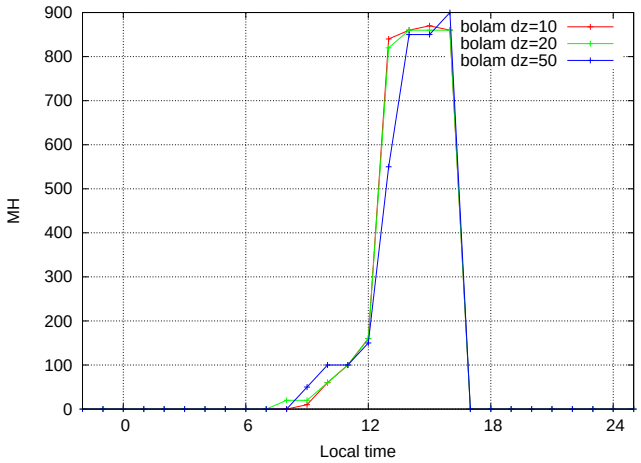

Figure A.8: Time series of the simulated mixing height (m) with different vertical resolutions, since 2200 LT 22 October, for 27 hours.

Bibliography

Beljaars, A. C. M. and A. A. M. Holtslag, 1991: Flux parameterization over land surfaces for atmospheric models. *Journal of Applied Meteorology*, **30**, 327–341.

Beyrich, F., 1997: Mixing height estimation from sodar data: a critical discussion. *Atmospheric Environment*, **31**, 3941–3954.

Blackadar, A. K., 1962: The vertical distribution of wind and turbulent exchange in a neutral atmosphere. *Journal of Geophysical Research*, **67 (8)**, 3095–3102.

Bougeault, P. and P. Lacarrere, 1989: Parameterization of orography-induced turbulence in a mesobetascale model. *Monthly Weather Review*, **117**, 1872–1890.

Brown, A. R., R. J. Beare, J. Edwards, A. Lock, S. J. Keogh, S. F. Milton, and D. N. Walters, 2008: Upgrades to the boundary-layer scheme in the Met Office numerical weather prediction model. *Boundary-layer Meteorology*, **128**, 117–132.

Canuto, V. M., Y. Cheng, and A. M. Howard, 2007: Non-local ocean mixing model and a new plume model for deep convection. *Ocean modelling*, **16**, 28–46.

Canuto, V. M., F. Minotti, C. Ronchi, R. M. Ypma, and O. Zeman, 1994: Second-order closure PBL model with new third-order moments: comparison with LES data. *Journal of the Atmospheric Sciences*, **51 (12)**, 1605–1618.

Caporaso, L., A. Riccio, F. Di Giuseppe, and F. Tampieri, 2013: Relating mean radiosounding profiles to surface fluxes for the very stable boundary layer. *Boundary-layer Meteorology*, **147**, 203–215.

Cheng, Y., V. M. Canuto, and A. M. Howard, 2005: Nonlocal convective PBL model based on new third- and fourth-order moments. *Journal of the Atmospheric Sciences*, **62 (7)**, 2189–2204.

Deardorff, J. W., 1966: The counter-gradient heat flux in the lower atmosphere and in the laboratory. *Journal of the Atmospheric Sciences*, **23**, 503–506.

Deardorff, J. W., 1972: Theoretical expression for the countergradient vertical heat flux. *Journal of Geophysical Research*, **77 (30)**, 5900–5904.

Fleagle, R. G. and J. A. Businger, 1980: *An introduction to atmospheric physics. Second edition.* Academic Press, New York, 432 pp.

Frech, M. and L. Mahrt, 1995: A two-scale mixing formulation for the atmospheric boundary layer. *Boundary-layer Meteorology*, **73**, 91–104.

Garratt, J. R., 1992: *The atmospheric boundary layer.* Cambridge University Press, Cambridge, 316 pp.

Gryanik, V. M. and J. Hartmann, 2002: A turbulence closure for the convective boundary layer based on a two-scale mass-flux approach. *Journal of the Atmospheric Sciences*, **59 (18)**, 2729–2744.

Holtslag, A. A. M. and B. A. Boville, 1993: Local versus nonlocal boundary-layer diffusion in a global climate model. *Journal of Climate*, **6**, 1825–1842.

Kader, B. A. and A. M. Yaglom, 1990: Mean fields and fluctuation moments in unstably stratified turbulent boundary layers. *Journal of Fluid Mechanics*, **212**, 637–662.

Kershaw, R. and D. Gregory, 1997: Parametrization of momentum transport by convection. I: Theory and cloud modelling results. *Quarterly Journal of the Royal Meteorological Society*, **123 (541)**, 1133–1151.

Mironov, D. and B. Ritter, 2005: Parameterization of convection in the Global NWP System GME of the German Weather Service. *Proceedings of the HIRLAM/NetFAM Workshop on Convection and Clouds*, 68–72.

Pergaud, J., V. Masson, S. Malardel, and F. Couvreux, 2009: A parameterization of dry thermals and shallow cumuli for mesoscale numerical weather prediction. *Boundary-layer Meteorology*, **132**, 83–106.

Pietroni, I., S. Argentini, I. Petenko, and R. Sozzi, 2012: Measurements and parametrizations of the atmospheric boundary-layer height at Dome C, Antarctica. *Boundary-layer Meteorology*, **143**, 189–206.

Seibert, P., F. Beyrich, S.-E. Gryning, S. Joffre, A. Rasmussen, and P. Tercier, 2000: Review and intercomparison of operational methods for the determination of the mixing height. *Atmospheric Environment*, **34**, 1001–1027.

Soares, P. M. M., P. M. A. Miranda, A. P. Siebesma, and J. Teixeira, 2004: An eddy-diffusivity/mass-flux parametrization for dry and shallow cumulus convection. *Quarterly Journal of the Royal Meteorological Society*, **130 (604)**, 3365–3383.

Stull, R. B., 1988: *An introduction to boundary layer meteorology*. Kluwer Academic Publishers, London, 666 pp.

Svensson, G., et al., 2011: Evaluation of the diurnal cycle in the atmospheric boundary layer over land as represented by a variety of single-column models: The second GABLS experiment. *Boundary-layer Meteorology*, **140**, 177–206.

Tiedtke, M., 1989: A comprehensive mass flux scheme for cumulus parameterization in large-scale models. *Monthly Weather Review*, **117**, 1779–1800.

Troen, I. and L. Mahrt, 1986: A simple model of the atmospheric boundary layer: sensitivity to surface evaporation. *Boundary-layer Meteorology*, **37**, 129–148.

Acknowledgment

I would like to express my sincere gratitude to Enrico Di Muzio, my friends and all the people that made me feel part of the CNR's family.